Early Steps of Ribosome Assembly Studied by Single Molecule Force Measurements

Lena Melkonyan

THÈSE DE DOCTORAT

de l'Université de recherche Paris Sciences et Lettres
PSL Research University

Préparée à l'école supérieure de physique et chimie industrielle

Early stages of ribosome assembly, studied by single-molecule force measurements

Les premières étapes de l'assemblage du ribosome, étudiées par mesure de force sur molécule unique

Ecole doctorale n°564

Physique en Ile-de-France

Spécialité Physique

COMPOSITION DU JURY :

M. Berry Richard
Université d'Oxford, Rapporteur

M. Wuite Gijs
VU Amsterdam, Rapporteur

M. Allemand Jean-Francois
ENS Paris, Membre du jury

Mme. Bassereau Patricia
Institut Curie, Membre du jury

M. Bockelmann Ulrich
ESPCI, Membre du jury

M. Ueda Takuja
Université de Tokyo, Membre du jury

Soutenue par Lena **Melkonyan**
le 13 décembre 2018

Dirigée par **Ulrich Bockelmann**

Confidentiel **31.05.2019**

ESPCI PARIS
EDUCATION SCIENCE INNOVATION

PSL
RESEARCH UNIVERSITY PARIS

Acknowledgements

For the success of this work, I want to thank my PhD adviser Ulrich Bockelmann, for his support, patience, understanding and many fruitful discussions we had during these three years.

I would like to thank the members of the jury, Patricia Bassereau, Takuya Ueda, Jean François Allemand, Ulrich Bockelmann and especially the two referees, Gijs Wuite and Richard Berry for interesting discussions during the defense.

I would like to thank prof. Robert Menard and Maryse Brandt for their kindness and efficient support in finding a room for my PhD defense. Especially Maryse Brandt, for her efficiency, kindness and very nice human qualities.

I would like to thank my colleagues and friends: Thierry Bizebard for sharing his vast knowledge in molecular biology, for the preparation of DNA and RNA duplexes, for giving me insight into ribosomal proteins and their manipulation, and for being always available for a discussion. Andreas Biebricher for checking some of my results in the Peterman lab in the University of Amsterdam, for many useful discussions and experimental insights into optical tweezers. Mathilde Bercy for forming me in optical tweezers, preparation of the molecular construct, for her friendship and her support in difficult moments. Ismaïl Cissé for sharing with me his knowledge in molecular biology technics, for many interesting, entertaining discussions, for his friendship and his precious human qualities. Laurent Geffroy for his patience and help in finding good experimental configurations and alining the optical tweezers, for interesting and friendly discussions. Kokoura Mensah for taking care of me as his younger sister, for his sensitivity, attention, support and his successes in cheering me up. Jyoti Prakash for his very entertaining character, for numerous interesting stories about culture, habits, family values and nature of Nepal and India. Stefan Rouach for being friendly and supportive. Mehdi Vahdati for his friendship, support and comprehension. Artem Kovalenko for his friendship, support and sharing our cultural experiences. Armand Hakopian for his friendship, support, attention and warm heartedness.

I would also like to thank my family: Kay Wiese, my husband, for his love, patience, support, understanding and for always believing in me and giving me motivation to go forward in life. Lili Melkonyan, my three yers old niece, for her love, cheerfulness, tenderness and kindness, for being able to make my whole day with her smile. Vahan Melkonyan and Mariam Grigoryan, my brother and my sister in law, for their love, cheerfulness, kindness, support and help in difficult moments. Margarit and Varuzhan Melkonyan, my mother and my father, for their love, support and comprehension, for all

the efforts they have taken to make me the person I am with my current achievements, for their eternal patience and for their faith in me.

Contents

Introduction

Dear reader, this work aims at a better understanding of two problems that are important, both from the point of view of fundamental physics, as of biology: First, the mechanical and structural behavior of biomolecules under an applied external force, and second, the early steps of ribosome assembly in *Escherichia coli (E. coli)*.

Let us remind that forces play important roles in biology. They are exerted on DNA, RNA and hybrid molecules by molecular motors and enzymes [1, 2, 3, 4, 5] during biological processes, as DNA replication, homologous recombination, strand-repair, packaging, transcription, ribosome assembly, translation, cell division, and many more. These forces can result in topological, conformational or structural changes inducing extension, torsion or generation of a single strand. The latter is particularly important for biological processes, as it can lead to parasitic interactions and formation of non-native structures, which may affect biological processes involving duplexes composed of DNA or RNA. Therefore, the understanding of the mechanical response of DNA and RNA duplexes, as well as of DNA-RNA heteroduplexes (DNA-RNA hybrids) to an applied force is not only a fundamental problem in physics, but also of vital interest for biology. Beyond providing insight into molecular and cellular regulation, it may be useful for the development of applications in biotechnology and medecine.

Our second motivation is to better understand ribosome assembly. The ribosome is responsible for protein synthesis in all living organisms. The ribosome consists out of two subunits, a *large* and a *small* one. Here we study the large one. It is formed out of two RNA strands called 23S with 2904 nucleotides and 5S with 120 nucleotides, and proteins. The standard view is that 23S folds immediately after it is synthesised, that proteins are incorporated right away, and that the absence of proteins prevents it to fold properly. A key indication for this view is the large difference in efficiency of ribosome assembly *in vivo* as compared to that *in vitro*. While ribosome biogenesis *in vivo* can occur efficiently at 37°C in a couple of minutes, reconstruction of ribosomes *in vitro* takes much longer: As an example, the large subunit folds in 90 minutes at 50°C. Two major reasons have been put forward to explain this difference. One is that non-ribosomal factors are present *in vivo* that transiently interact with the nascent ribosome and assist its assembly. The second one is that *in vivo* ribosomal proteins and assembly factors bind to the RNA during its synthesis, facilitating its folding.

The idea of our experiment is the following: Using an RNA-DNA hybrid, we liberate the RNA with the sequence of the ribosomal RNA (i.e. 23S and 5S) at the rate at which it is synthesized in the cell, namely 40 base pairs per second. In this way we mimick as

closely as possible RNA synthesis in living organisms, while at the same time keeping full control over the environment. More specifically, we compare folding of the rRNA in our standard buffer alone with the buffer augmented by the five proteins which are believed to bind first (early binders) [6]. This comparison is achieved by studying the force-extension curves in our optical tweezer experiments. Incorporation of the proteins is visible as a change in the hysteresis of the measured force-extension curves.

More specifically we ask ourselves the following questions:

Problem 1.

What are the mechanical responses of deoxyribonucleic acid (DNA), ribonucleic acid (RNA) duplexes and DNA-RNA heteroduplexes to applied external forces? What is the difference between the response of different molecular duplexes?

Problem 2.

What is the effect of early binding ribosomal proteins uL4, uL24, uL22, uL13, bL20 on early steps of ribosome assembly?

These two questions will be treated in chapters I and II of the manuscript, respectively. In chapter I we also present the molecular objects of the study, the experimental setup and afterwards the way to prepare the molecular constructs for the single-molecule force measurements. A summary in French is given in chapter III. Detailed protocols are provided in the annex A.

Chapter I

Overstretching molecular duplexes made of DNA and RNA

In this work, we apply force on DNA and RNA duplexes, as well as DNA-RNA hybrids. In order to better understand the mechanical properties and force-induced structural modifications of these biopolymers, let us first refresh our knowledge on their chemical and physical structures.

I.1 DNA, RNA, DNA-RNA hybrid

I.1.1 Chemical structure

DNA

DNA is one of the main fundamental functional biopolymers and the only permanent carrier of genetic information in the cell. In native structure it is a double stranded helical molecule, each strand of which represents a polypeptide chain with a sequence of four different nucleotides called Adenine (A), Guanine (G), Cytosine (C), and Thymine (T). Each nucleotide consists of three different chemical groups: A phosphate group, 5 carbon sugars (deoxyribose for DNA) and a nitrogenous base, the latter being the only group by which the four nucleotides differ from each other. By establishing covalent bonds between the phosphate group of one and the sugar group of the other, these nucleotides form a single polypeptide chain of deoxyribonucleic acid (DNA) with a sugar-phosphate backbone and bases attached to it. Two DNA strands are joined together via hydrogen bonds between the bases of one strand and their complementary bases on the other strand forming base pairs. Adenine is always paired with Thymine (AT base pair) and Guanine with Cytosine (GC base pair). Two consecutive base pairs are held together by stacking interactions, see figure I.1.

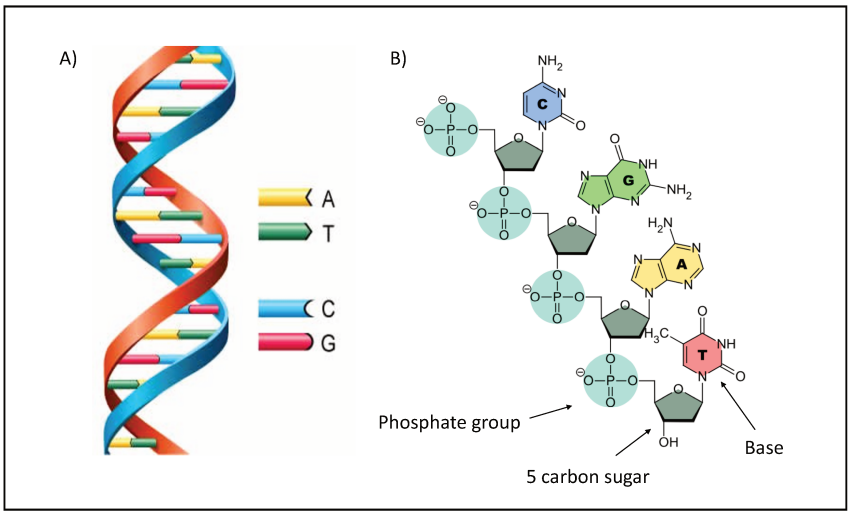

Figure I.1: A) Schematic representation of a double stranded DNA helix and its four nitrogenous bases: adenine (yellow), thymine (green), cytosine (cyan), guanine (red). B) Chemical structure of the four DNA nucleotides. Each nucleotide consists of a phosphate group, five carbon sugars, and a base, either cytosine (blue), guanine (green), adenine (yellow), or thymine (red).

RNA

Similar to DNA, RNA is functional in the cell. It plays important roles in different biological processes, like ribosome assembly, protein synthesis, gene regulation, gene expression and so on. Unlike DNA, RNA appears in the cell mainly single stranded. Similar to a single strand of DNA (ssDNA), a single strand of RNA (ssRNA) is a polypeptide chain composed of a sequence of four nucleotides: adenine, guanine, cytosine and uracil instead of thymine, see figure I.2. As in DNA, the latter can bind together by covalent bonds in a sequential manner forming AU and GC pairs. This allows to represent RNA, like DNA, as a sequence of nitrogenous bases attached to a long sugar-phosphate backbone. However, there is a difference in sugar groups. In RNA this sugar group is ribose unlike deoxyribose in DNA, see figure I.3. To protect its hydrophobic bases, an RNA strand interacts with itself forming hydrogen bonds between complementary bases. This results in a secondary structure composed of loops and double helical regions.

DNA-RNA hybrid

Due to many similarities in their chemical structure, DNA and RNA can form double helices similar to DNA. These *hybrids* are involved in homologous recombination of chromosomal DNA in case of double-strand DNA damage [7, 8]. DNA-RNA hybrids consist of one DNA and one RNA strand bound to each other by hydrogen bonds

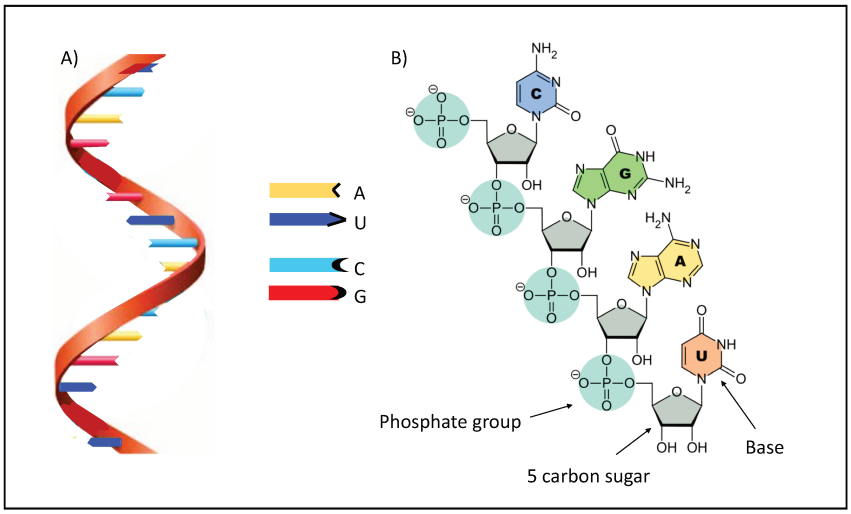

Figure I.2: A) Schematic representation of single stranded RNA and its four nitrogenous bases: adenine (yellow), uracil (blue), cytosine (cyan), guanine (red). B) Chemical structure of four RNA nucleotides. Each nucleotide consists of a phosphate group, a 5 carbon sugar and a base (cytosine (blue), guanine (green), adenine (yellow), uracil (orange).

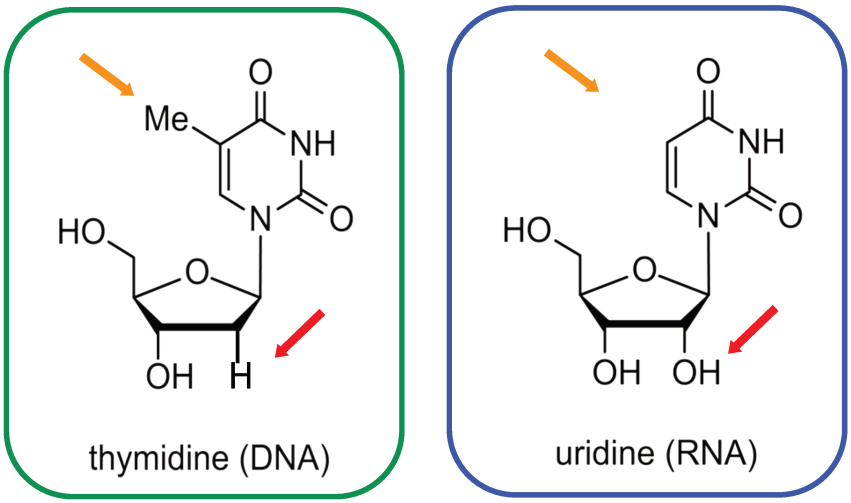

Figure I.3: Chemical structure differences between thymine and uracil bases and between 5 carbon sugars of DNA and RNA molecules. Thymine and uracil differ by a methyl group, which is present in thymine and absent in uracil (orange arrows). The OH group at the second position of the RNA 5 carbon sugar is replaced by a hydrogen atom in DNA (red arrows).

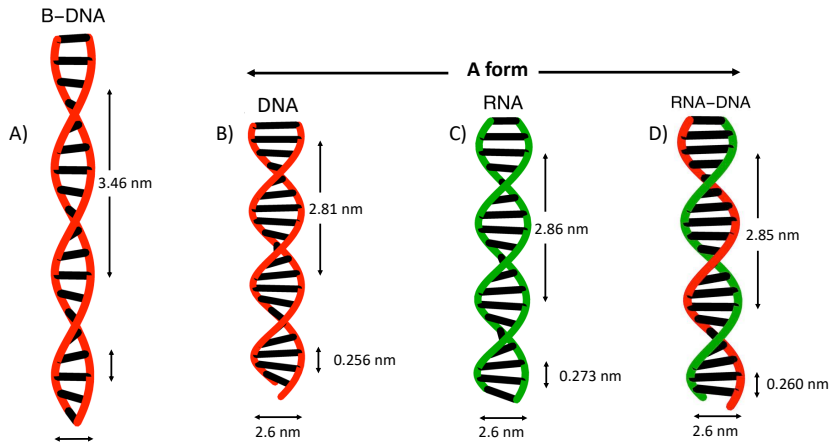

Figure I.4: Physical structures of dsDNA, dsRNA, RNA-DNA hybrid and differences of A and B form helices. In double stranded configuration all three molecules exhibit helical structure. Depending on external conditions dsDNA adopts A or B form, whereas dsRNA and RNA-DNA adopt only A form. Both A and B form helixes are right handed. Compared to B form, helixes in A form are shorter and wider. A) B-DNA has 2nm diameter and a distance of 0.346nm between two consecutive base pairs. One helical turn is 3.46nm corresponding thus to 10 base pairs. B) A-DNA has a diameter of 2.6nm and a distance between two consecutive base pairs is 0.256nm. One helical turn is 2.81nm corresponding thus to 11bp. C) A-RNA double helix has 2.6nm diameter and 0.273nm distance between two consecutive base pairs. One helical turn is 2.86nm corresponding thus to 10.5bp. D) RNA-DNA hybrid has 2.6nm diameter and 0.26nm distance between two consecutive base pairs. One helical turn is 2.85nm corresponding thus to 11bp.

between complementary bases, forming thus three different base pairs along the hybrid sequence: AT, GC, and AU, see figure I.4. As we saw above, all three molecules form, either completely or partially, a double helical structure in their native state. Let us see how similar and how different they are.

I.1.2 Physical structure

At room temperature, neutral pH and above 75% humidity, dsDNA is a double helix of B form (Fig. I.4A). It is right-handed with 2nm diameter and a helical turn of 3.46nm which corresponds to 10 base pairs. The distance between two adjacent base pairs is 0.346nm.

Compared to dsDNA, dsRNA and RNA-DNA hybrids are in A form. As one can see from Fig. I.4, unlike the B form which is thin and long, double helixes in A form are short and wide. A helix formed by dsRNA has a diameter of 2.6nm. The distance between two adjacent base pairs is 0.273nm. One complete helical turn is 2.86nm

corresponding to 11 base pairs per turn. The double helical structure of RNA-DNA hybrid is very close to that of dsRNA. It has a diameter of 2.6nm. The distance between adjacent base pairs is 0.26nm. One complete helical turn is 2.85nm corresponding to 10.5 base pairs per turn.

I.2 Optical tweezers

I.2.1 The principle of optical trapping

Over the last decade many different tools and techniques were developed to study the biological role and the mechanical properties of single molecules. Among them, dual-beam optical tweezers are of particular interest. Their principal is simple, and based on light-matter interaction. In our case, there is interaction between a focused laser beam and a polystyrene bead.

Comparing the wavelength of the laser, and the size of the object to be trapped, there are three regimes:

1. $\lambda \gg d$, the wavelength of light λ is large as compared to the size d of the object (dipole-approximation regime).

2. $\lambda \ll d$, the wavelength of light λ is small compared to the size d of the object (ray-optics regime).

3. $\lambda \approx d$, the wavelength of the light λ is comparable to the size d of the object.

In our experiments we deal with case 3, $\lambda \approx d$, which is well described by the generalized Lorentz-Mie theory [9]. In order to understand the basic principle of optical trapping and avoid complicated mathematics, we restrict our considerations to case 2, i.e. $\lambda \ll d$.

Light carries momentum, and as we know in scattering experiments the total momentum is conserved. When interacting with matter, the photons of the laser beam are partially reflected and refracted by the matter thus loosing momentum. Let us denote by $\vec{p}$ the momentum of the photons before their interaction with the bead, by $\vec{p}_1$ the momentum of those which have been refracted, and by p_2 the momentum of those reflected by the bead. Then, the change in photon momentum, i.e., the momentum that the photons transfer to the bead due to their interaction, is

$$\frac{d\vec{p}}{dt} = \vec{p}_1 + \vec{p}_2 - \vec{p}\,. \tag{I.1}$$

As stated, this difference is partially due to refraction and partially due to reflection of the photons. Thus, it can be represented as a sum of the momentum changes of the photons, due to refraction dp_{refr}/dt and reflection dp_{refl}/dt.

$$\frac{d\vec{p}}{dt} = \frac{d\vec{p}_{\text{refr}}}{dt} + \frac{d\vec{p}_{\text{refl}}}{dt} \tag{I.2}$$

According to Newtons second law, the force transferred to the bead is

$$\frac{d\vec{p}}{dt} = \vec{F} \ . \tag{I.3}$$

Therefore equation (I.2) can be written as

$$\vec{F} = \vec{F}_{\text{grad}} + \vec{F}_{\text{scat}} \ . \tag{I.4}$$

In equation (I.4) force $\vec{F}_{\text{grad}}$ corresponds to the force induced by the refracted lite and the force $\vec{F}_{\text{scat}}$ is the force induced by the reflected lite. and For a *Gaussian* laser beam, the beam intensity is well approximated by a Gauss-function, and thus is highest in the center. If the bead is in the periphery of an unfocused laser (Fig. I.5a), the force $\vec{F}_{\text{b}}$ induced on the bead by beam b coming from the center dominates over the force $\vec{F}_{\text{a}}$ induced by the beam coming from the periphery. As beam b is refracted to the top, the resultant force $\vec{F}_{\text{grad}}$ will be directed down towards the center of the laser beam. It will thus move the bead to the center, while at the same time moving it in the direction of the incoming laser beam.

There is another force component acting on the bead. It is the scattering force $\vec{F}_{\text{scat}}$, induced by the reflection of photons. Being directed along the propagation of the laser beam, $\vec{F}_{\text{scat}}$ moves the bead along the laser beam. According to equation (I.4), the resultant force $\vec{F}$, which is the sum of $\vec{F}_{\text{grad}}$ and $\vec{F}_{\text{scat}}$, will attract the bead to the center of the beam and move it along its propagation axis.

Let us now consider a focused laser, see Fig. I.5b. If the bead is in the center of the beam, the forces $\vec{F}_{\text{a}}$ and $\vec{F}_{\text{b}}$ are equal in magnitude. They result in a force $\vec{F}_{\text{grad}}$ antiparallel to the direction of propagation of the beam, becoming therefore a force counteracting $\vec{F}_{\text{scat}}$. While $\vec{F}_{\text{scat}}$ moves the bead along the laser beam, $\vec{F}_{\text{grad}}$ moves the beads towards the focal point, i.e., the point with the highest light intensity. This way the bead is stably trapped slightly behind the focal point [10, 11]. Another way to understand this is to realise that due to focussing, the incoming beam comes "from the side", thus rotating the axes of the refracted beam s.t. it obtains a component moving in the opposite direction of the incoming beam.

I.2.2 Dual beam optical tweezers

To do our experiments we used dual beam optical tweezers (Fig. I.6). The laser beam emitted by a Nd:YVO_4 laser (1064nm, 10W) is first enlarged in diameter by a telescope composed of lenses L1 and L2. This allows us to reduce heating of the following optical components. The laser beam is then split into two independent beams of perpendicular polarization by a polarizing cube C1. A half wave plate $\lambda/2$ allows us to adjust the repartition of the power among the splited beams. One of the resulting beams is reflected by a mirror attached to a piezoelectric tilting stage creating a mobile beam. The other beam is reflected by a stable mirror, creating a fixed beam. After being recombined by a second polarizing cube C2, the two beams pass through a high-numerical aperture microscope objective (Nikon, 100x oil immersion, NA = 1.4)

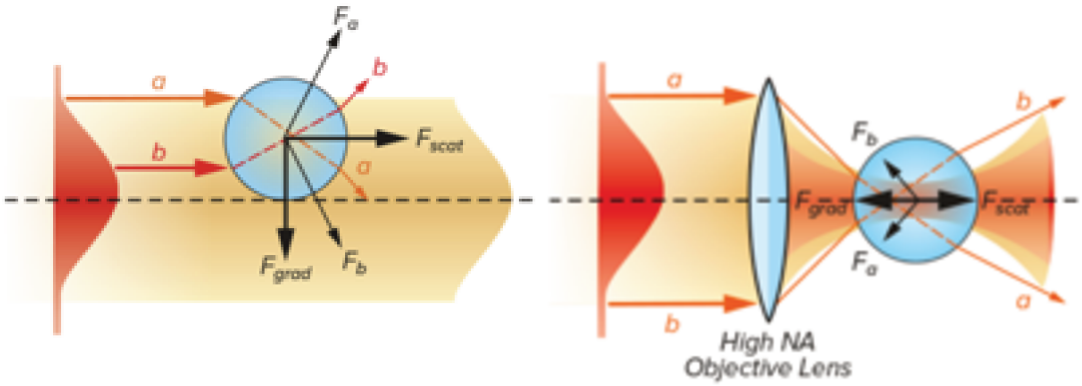

Figure I.5: Optical trapping phenomenon in ray optics. Interacting with a bead, rays a and b induce forces F_a and F_b on the bead. The figure is taken from optical nanomaipulation lab (ONM) web page.

creating a fixed trap and a mobile trap in the sample plane. The lateral distance between the fixed and mobile trap can be adjusted with nanometer precision. After passing through the sample, the two beams are collimated by a second objective (Nikon, 60x water immersion, NA = 1.2). The mobile beam is separated using a Glan air polarizer and blocked by a beam blocker. This way, only the fixed beam reaches the detector. We use a position-sensitive diode (PSD) as detector to measure the position of the bead within the fixed trap using back-focal-plane interferometry. The force is derived from the position of the bead within the trap. The power spectral density of the bead is measured to calibrate the force, using a procedure described elsewhere [12].

I.3 Four molecular constructs

To study the force response of DNA and RNA double strands and hybrids, we prepared four different molecular constructs (Fig. I.7): dsDNA (Fig. I.7a), dsRNA (Fig. I.7b), RNA-DNA hybrid (Fig. I.7c) and DNA-RNA hybrid (Fig. I.7.d). Three extremities of each molecular construct are modified by incorporation of biotin-carrying nucleotides and one extremity is left unmodified. Since biotin makes a strong non-covalent bond with streptavidin, the incorporation of biotin-carrying nucleotides allows us to attach three extremities of the molecule to beads. The unmodified extremity will have no attachment and thus remains free. The two beads are then trapped in two optical tweezers and moved apart. This way, forces are exerted on the molecule spanning them (Fig. I.8).

All four molecular constructs have the same length (4050bp) and the same sequence of nucleotides. For further scientific study of ribosome assembly of E.coli described in section II of this manuscript, the molecules were prepared such that the leading strand with one attachment (at the 3' end) to a bead carries in consecutive manner (from 5' to 3') the genes rrlB (coding for 23S ribosomal RNA), rrfB (coding for 5S rRNA) and half

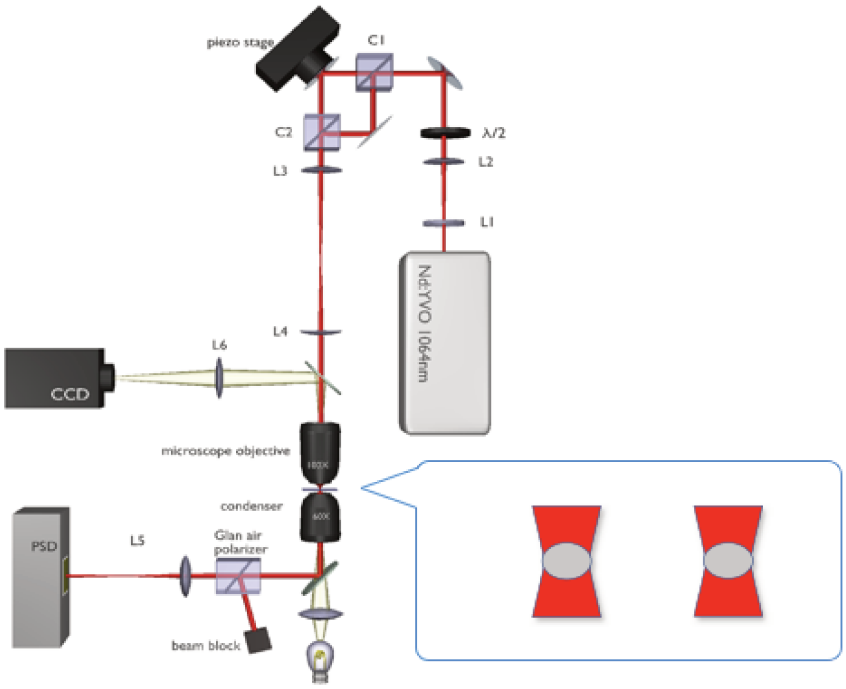

Figure I.6: Schematic representation of the major elements of our dual beam optical tweezers setup. In the inset, we show two beads trapped in the fixed and mobile traps.

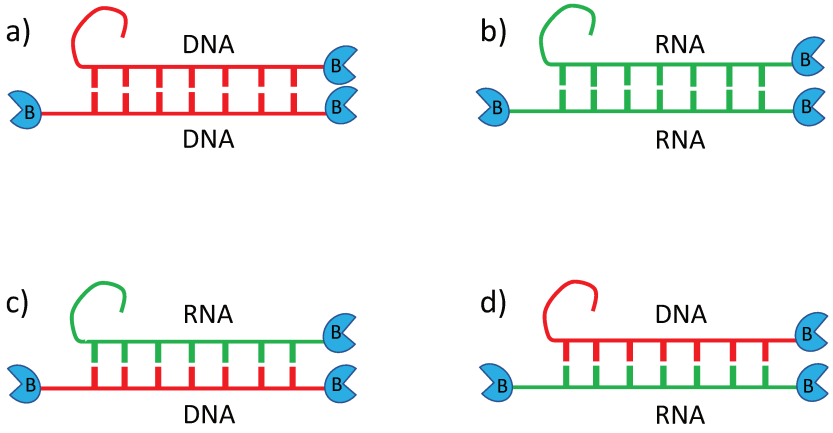

Figure I.7: Schematic representations of four molecular constructs and their attachment sites. DNA strands are shown in red, RNA strands in green. Biotin groups are represented in blue. Three of the four extremities of each molecule have biotin-modified nucleotides, while one extremity has no modification. a) doubled stranded DNA (dsDNA), b) double stranded RNA (dsRNA), c) RNA-DNA hybrid (RNA-DNA), d) DNA-RNA hybrid (DNA-RNA). Note the difference between the RNA-DNA hybrid and the DNA-RNA hybrid. In the former (latter) case the DNA (RNA) strand will be under tension.

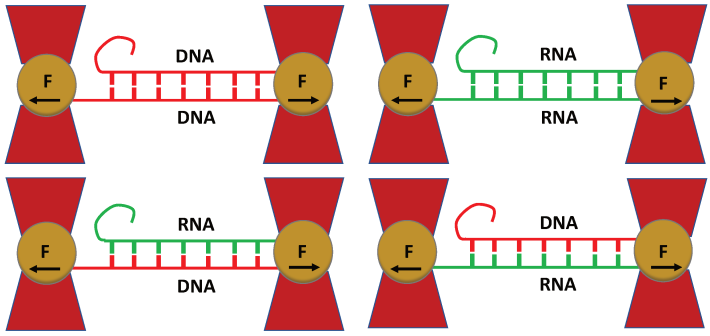

Figure I.8: Schematic representation of four molecules, as they are optically trapped in the centers of two focused laser beams. As in the preceding figure, DNA and RNA strands are red and green, respectively. Arrows indicate the direction of displacement of the laser beams. The force F exerted by the optical trap on the bead is represented.

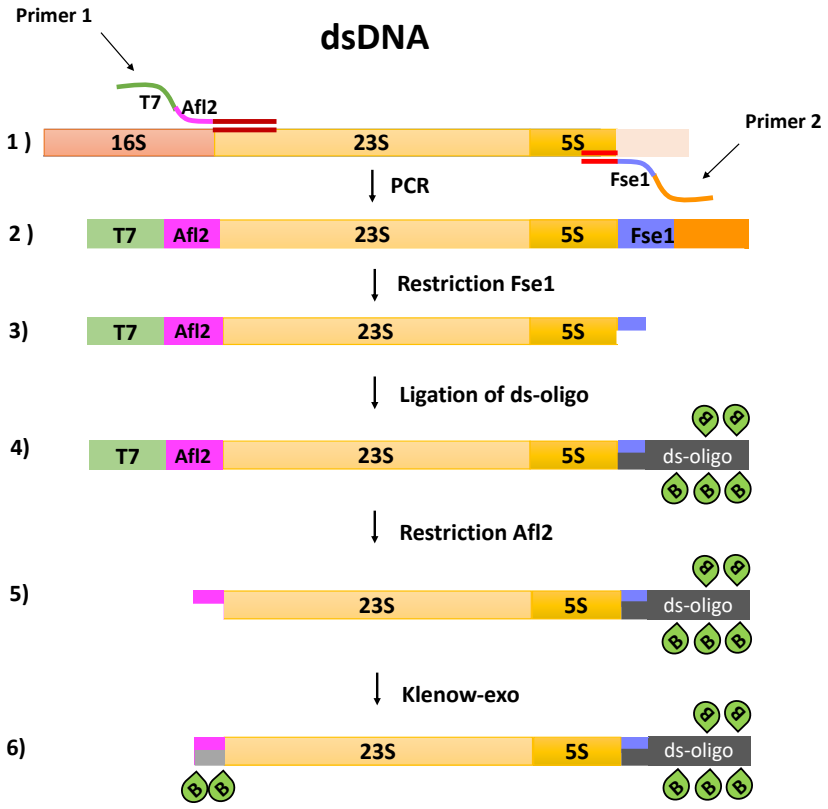

Figure I.9: Preparation of dsDNA

of murB, where murB plays the role of a spacer. The total length of our constructs is well-adapted for single-molecule manipulation, in particular it is convenient to capture the two beads linked by a molecule of this length (4050bp) in separate traps. We now describe the detailed steps needed to prepare the constructs, first for dsDNA, then for the RNA-DNA hybrid, dsRNA and for the DNA-RNA hybrid at the end.

I.3.1 Preparation of dsDNA

The sequence of interest is amplified by a polymerase chain reaction (PCR) from the plasmid pT7rrnB (Fig. I.9). The PCR primers (primer 1 and primer 2) were designed to introduce the sequence of a T7 polymerase promotor and an Afl2 restriction site (primer 1) at one extremity of the double-stranded PCR product, and the sequence of an Fse1 restriction site (primer 2) at the other extremity. The PCR product was then digested by the Fse1 restriction enzyme. The restricted piece was purified and replaced by a similar sequence carrying biotin via ligation. The resultant product was then digested by an Afl2 restriction enzyme generating a 4-nucleotide overhang at the 5' end of the leading strand. The complementary nucleotides were filled in by Klenow DNA polymerase (Klenow exo-fragment). Some of them carry biotin groups

for attachment.

I.3.2 Preparation of the RNA-DNA hybrid

As for dsDNA, the sequence of interest was first amplified by a polymerase chain reaction (PCR, step1 Fig. I.10). The PCR primers (primer 1 and primer 2) were designed to introduce the sequence of a T7 polymerase promotor and an Afl2 restriction site (primer 1) at one extremity of the double-stranded PCR product, and the sequence of an Fse1 restriction site (primer 2) at the other extremity (Fig. I.10, step 2). A part of the PCR product (2μg) was conserved at $-20°$C for in vitro RNA transcription and the rest was used to prepare dsDNA with biotin modifications at three of its extremities following the same steps (Figures N5, N6, steps 3-6) as described in section I.3.1. Once the dsDNA with biotin modifications was ready (Fig. I.10, step 6), the conserved PCR product was used to obtain in vitro transcribed RNA containing the sequences of 23S and 5S rRNAs (Fig. I.10, step 7). It is important to prepare fresh RNA for this step, since its stability is low and it degrades fast as compared to DNA. After preparation of ssRNA (Fig. I.10, step 7), the RNA and the dsDNA (Fig. I.10, step 6) were combined to do a strand exchange. This way, many copies of the RNA-DNA hybrid with biotin modifications at the two extremities of the DNA strand were obtained (Fig. I.10, step 8). The last biotin modification at the 3rd extremity of the RNA-DNA construct (3' end of RNA strand) was introduced by a small RNA oligo of 20bp carrying two biotin-dT at its extremity. The remaining dsDNAs were degraded by an appropriate restriction enzyme to make sure that all the measurements were done on RNA-DNA hybrids only.

I.3.3 Preparation of dsRNA

Each strand of dsRNA was prepared separately. The leading strand was prepared as described in the previous section I.3.2. (Fig. I.10, steps 1, 2, 7, Fig. I.11, steps 1, 2, 3). The preparation of the lagging strand was done as follows. The sequence of interest (23S and 5S rRNA) was amplified by a polymerase chain reaction (PCR). The PCR primers 3 and 4 (Fig. I.11, step 1) were designed to introduce a random sequence at one extremity of the PCR product and a sequence of T7 polymerase promoter and a restriction site for FseI restriction enzyme at the other extremity of the PCR product (Fig. I.11, step 5). As one can see from Fig. I.11, to prepare the lagging strand the T7 polymerase promotor sequence is introduced at the opposite extremity of the PCR product (Fig. I.11, step 5) as compared to the preparation of the leading strand (Fig. I.11, step 2). After the PCR reaction, part of it was used to perform in vitro transcription of the lagging single stranded RNA (Fig. I.11, step 8). The latter was biotin-modified at both extremities via splint ligation. The idea of our particular splint ligation is the following. T4 RNA ligase 2 can ligate pieces of ssRNA (biotin-modified in our case) to DNA-RNA hybrids. This means that in order to ligate biotin-modified RNA oligonucleotides at two extremities of the ssRNA_lagg, it is necessary to create small regions of a DNA-RNA hybrid at both extremities. To do this, two DNA oligonucleotides (DNA1 and DNA2, Fig. I.11, step 7)

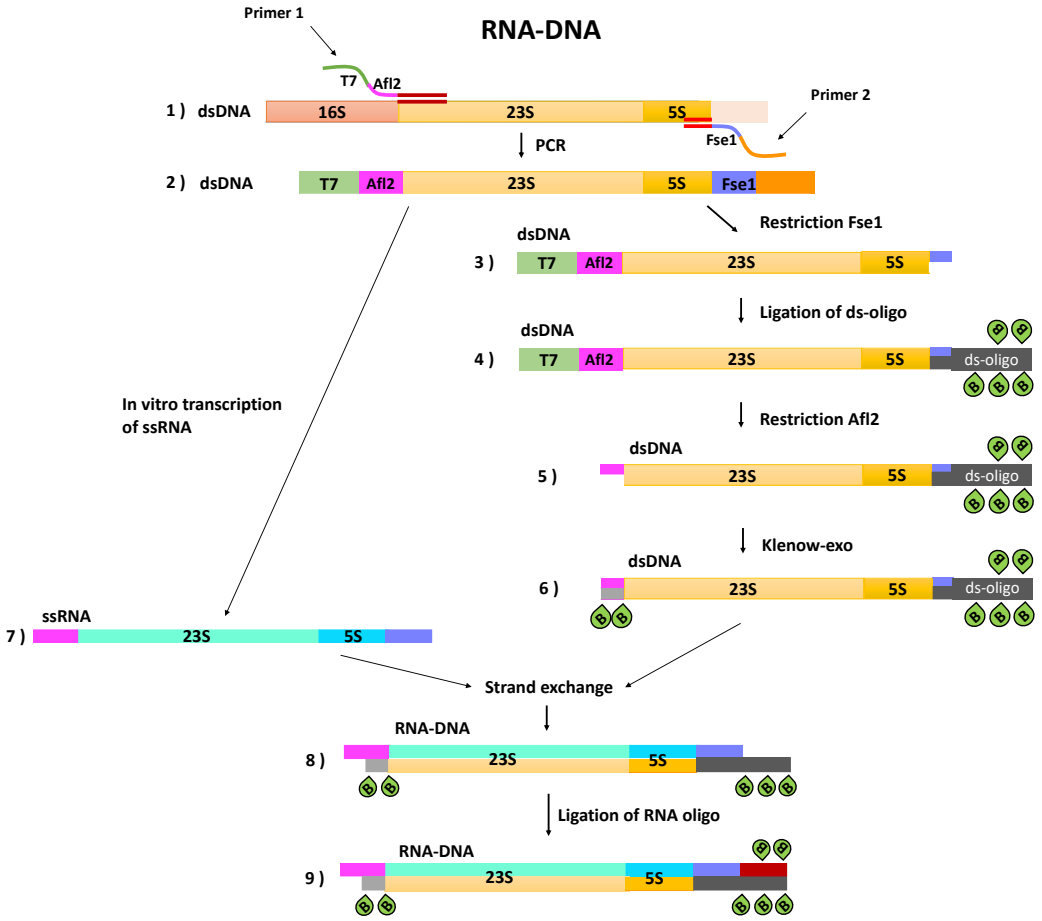

Figure I.10: Preparation of the RNA-DNA hybrid with biotin modifications.

having half of their sequence complementary to the ssRNA_lagg extremities and half to RNA oligonucleotides (biotin-modified) were hybridized to ssRNA_lagg, creating bridges for ligation of two RNA oligonucleotides (RNA1, RNA2, in red, Fig. I.11, step 9). After successful ligation, two RNA single strands (ssRNA_lead and ssRNA_lagg) were hybridized creating dsRNA with two biotin-modified edges (Fig. I.11, step 8). The final dsRNA construct with 3 biotin-modified extremities was obtained by ligation of the last RNA3 oligonucleotide (Fig. I.11, step 9). The latter is the same as for RNA-DNA hybrid (Fig. I.10, step 9).

I.3.4 Preparation of DNA-RNA hybrid

In this case, the leading strand is DNA and the lagging strand is RNA. The preparation of this construct is done in three steps: a preparation of dsDNA with three biotin-modified extremities (Fig. I.12, steps 1-5), preparation of the lagging RNA single strand with biotin modifications at its 5' and 3' ends (Fig. I.12, steps 6-9) and

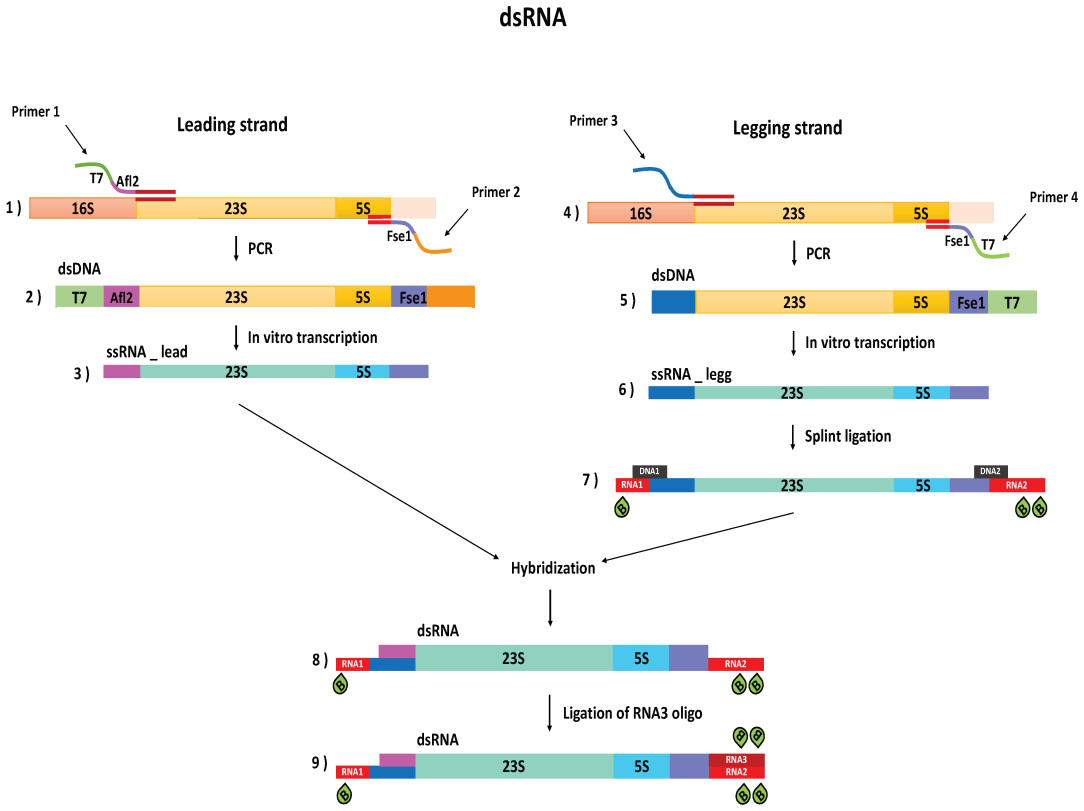

Figure I.11: Preparation of the dsRNA molecule with biotin modifications.

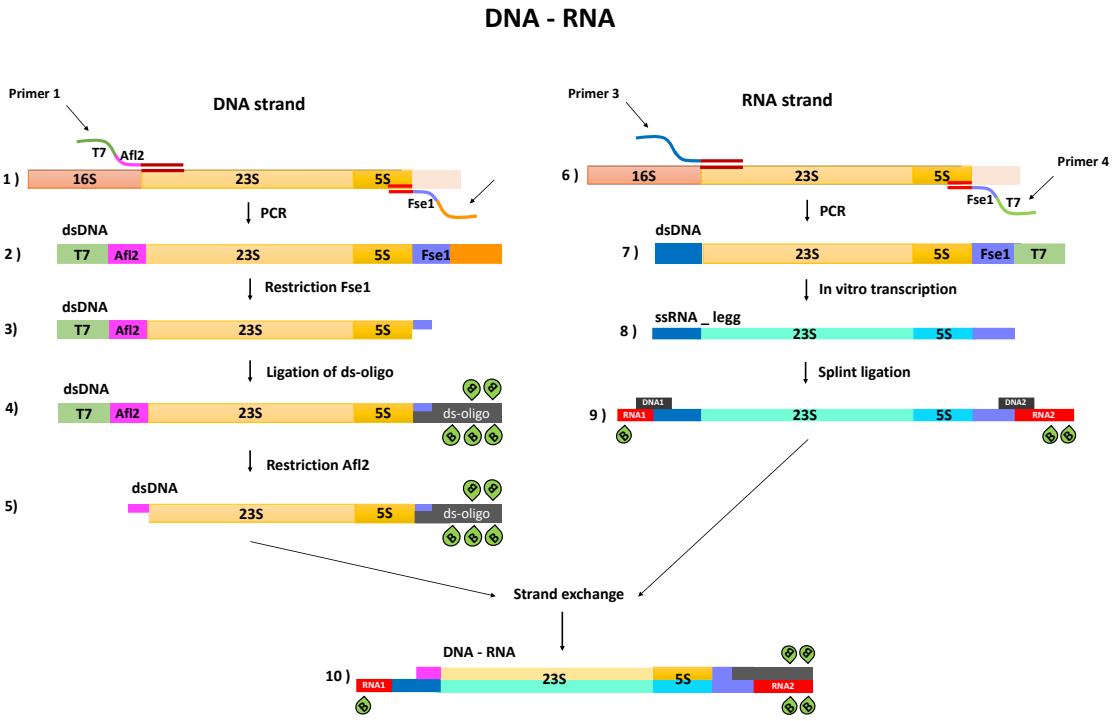

Figure I.12: Preparation of DNA-RNA hybrid with biotin modifications.

an exchange of the DNA-lagging strand by a RNA-lagging strand via a hybridization reaction (Fig. I.12, step 10). The preparation of dsDNA is the same as in section I.3.1 (Fig. I.12, steps 1-6) and the preparation of the lagging ssRNA is the same as described in section I.3.3 (Fig. I.11, steps 4-7).

I.3.5 Further treatment of the constructs

When the molecular constructs are prepared, part of them are conserved at $-20°C$ for later use, while part of them are mixed with streptavidin-coated polystyrene beads. The mixture is first centrifuged 6 min at 30G and then incubated at room temperature ($25°C$) for one hour. Centrifugation allows the beads and the molecules to come close together, thus increasing their binding efficiency and reducing the incubation time from 3 hrs to 1 h. After incubation, the sample is loaded into a fluidics chamber composed of two glass coverslips sealed together by 2 parallel parafilm layers. After loading with the molecular construct the two open edges of the chamber are sealed with wax (Fig. I.13).

Finally, the sample is installed on the microscope stage between two objectives (100x oil and 60x water, described above), a bead couple with a molecule attached in between is searched for, found, trapped and a force measurement is performed (Fig. I.14).

The results of these experiments are given in papers 1 and 2.

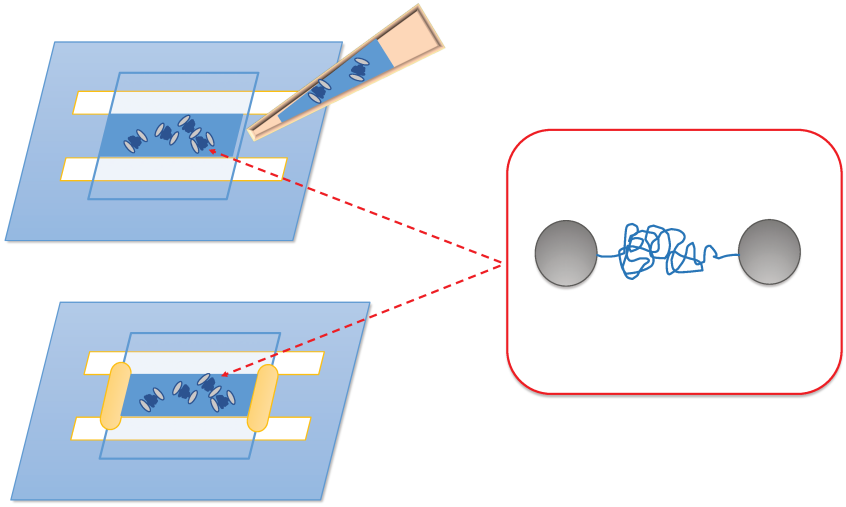

Figure I.13: Fluidics chamber composed of two glass coverslips sealed together by 2 parallel parafilm layers. The two open edges of the chamber are sealed with wax.

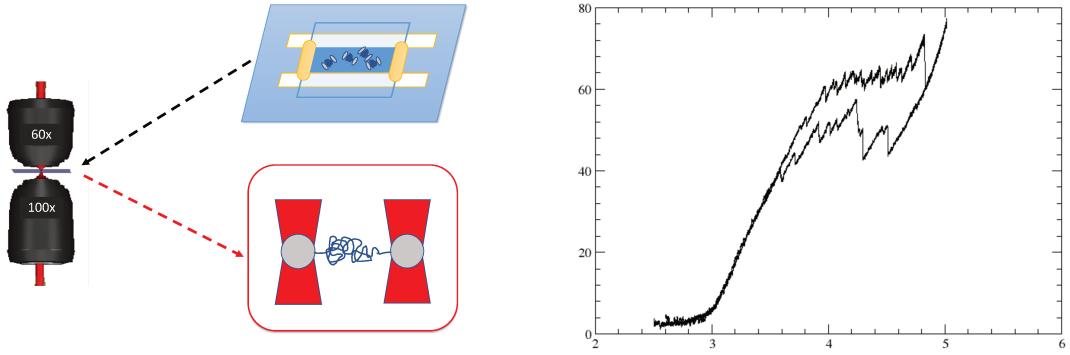

Figure I.14: Left: Schematic representation of the fluidics chamber in the optical trap. Right: Example of a force-extension curve. (Forces are in pN, extension in nm.)

Overstretching double-stranded RNA, double-stranded DNA and RNA-DNA duplexes

Submitted

L. Melkonyan[1], M. Bercy[1], T. Bizebard[2], and U. Bockelmann[1]

1 Nanobiophysique, ESPCI Paris
10 rue Vauquelin, 75005 Paris, France

2 Expression Génétique Microbienne,
IBPC, CNRS UMR 8261
13 rue Pierre et Marie Curie,
75005 Paris, France

Using single-molecule force measurements, we compare the overstretching transition of the four types of duplexes composed of DNA or RNA strands. Three of the four extremities of each double helix are attached to two microscopic beads and a stretching force is applied with a dual-beam optical trapping interferometer. We find that overstretching occurs for all four duplexes with small differences between the plateau forces. Double-stranded RNA (dsRNA) exhibits a smooth transition, in contrast to the other three duplexes that show sawtooth patterns, the latter being a characteristic signature of peeling. This difference is observed for a wide range of experimental conditions. We present a theoretical description, which explains the difference and predicts that peeling and bubble formation do not occur in overstretching dsRNA. Formation of S-RNA is proposed, an overstretching mechanism that contrary to the other two does not generate single strands. We suggest that this singular RNA property helps RNA structures to assemble and play their essential roles in the biological cell.

I. INTRODUCTION

Forces act on DNA and RNA in the biological cell. They induce elastic deformation and torsion, can give rise to conformational and structural transitions and sometimes lead to base pair opening as well as profound modifications in base stacking and tertiary interactions. Generation of single-strands from duplexes containing DNA or RNA strands is particularly important, since it can lead to parasitic interactions and non-native structures. These duplexes are ubiquitous in the cell. Besides the DNA double helix being composed of two complementary single strands, most RNA molecules contain numerous helical parts and many of these local duplexes are essential elements of native RNA structures. Moreover, hetero-duplexes of DNA and RNA occur in DNA replication, DNA transcription, gene regulation and gene editing systems.

It has been shown by single-molecule measurements that mechanical force can generate single strands in different ways. In the unzipping configuration, forces pull the two strands of one duplex extremity in opposite directions and mechanically separate them [1–3]. In the peeling configuration, which occurs around 60 pN in overstretching of topological open nucleic acid (NA) duplexes, forces act along the helical axis from opposite duplex extremities and one strand peels off in a shear mode [4]. DNA overstretching was discovered about two decades ago by single-molecule force measurements [5, 6]. The experimental observations triggered many studies and controver-

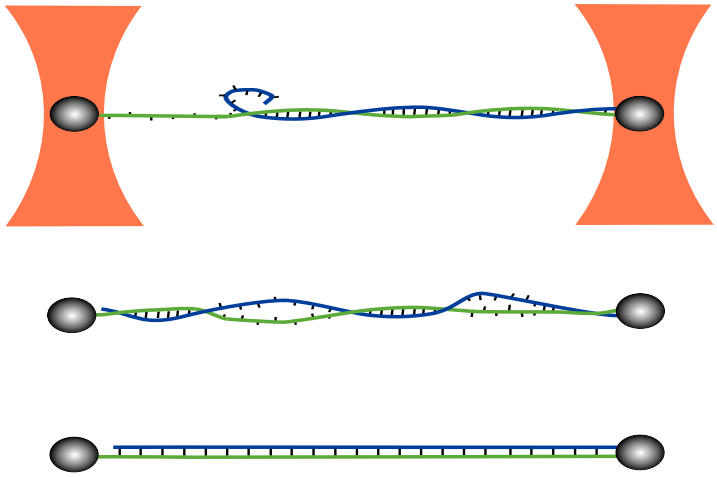

FIG. 1: Schematic representation of the measurement configuration and of the three overstretching mechanisms. The nucleic acid duplex is attached by three of its four single-strand extremities to two microscopic beads (beads and molecule are not at the same scale). The two beads of each dumbell are captured in separate optical traps (orange). Force versus displacement curves are obtained by measuring the position of one bead within the trap to nanometer precision, while the other trap is displaced. Peeling of the free strand, bubble formation and S-structure formation are presented from top to bottom. Single-strands under force and the S-structure exhibit a longer separation between adjacent nucleotides than the regular double helix. Base pairing is maintained in the S-structure, but base pair stacking and the number of helical turns are strongly reduced. Our molecular constructs are free to rotate around the axis of applied force, as on one side the bead is attached only to a single strand (green strand on the left-hand side of the figure).

sial discussions about the molecular mechanism underlying DNA overstretching, see [7, 8] and references therein. Recently, it has been shown experimentally that DNA overstretching can be caused by several mechanisms, including peeling, bubble formation as well as a structural transition from the B-form helix to an S-DNA structure [4, 8–10]. These mechanisms are schematically represented in Fig.1.

While overstretching by bubble formation and by transition to S-DNA both show smooth plateaus in the force versus extension curve, peeling induces a characteristic sawtooth-shaped pattern. A sawtooth-shaped pattern can be observed only in the presence of a peeling front in dsNA. This peeling front can be either a free extremity of one of two strands under tension or a nick along one of the strands [8]. The absence of any of the latter always leads to smooth overstretching [8]. The latter, can, however, be observed even when a peeling front is present, though special experimental conditions are required.

Here we investigate the overstretching transition of four different nucleic acid duplexes by single-molecule force measurements. These duplexes are double-stranded DNA (dsDNA), double-stranded RNA (dsRNA), a hetero-duplex with the DNA strand under tension (RNA-DNA) and a hetero-duplex with the RNA strand under tension (DNA-RNA), respectively. Strikingly, we find that dsRNA always exhibits a smooth overstretching signal, an observation that holds for a wide investigated range of salt conditions and pulling speeds. In contrast, the other three duplexes exhibit pronounced sawtooth-shaped signals during overstretching. Comparison between the experimental data and a theoretical description based on the assumption of local thermal equilib-

rium indicates that peeling and bubble formation do not occur for dsRNA. Towards the end of the manuscript, we briefly discuss under which circumstances the absence of these single-strand generating mechanisms could be important in the biological cell.

II. MATERIALS AND METHODS

A. Force measurement setup

Detailed descriptions of the dual-beam optical trapping interferometer and the sample preparation steps immediately preceding the force measurement are published elsewhere [11]. The linearly polarized beam of a CW Nd:YVO_4 laser (Millenia IR, Spectra-Physics, 1064 nm, 10W) is split with a polarizing cube beam splitter. One of the resulting beams is shifted in frequency by an acousto-optic frequency shifter. Then it is deflected by a piezoelectric mirror mount with an integrated position sensor operating in feedback loop and represents the mobile beam. The other beam remains fix. The two beams are combined with a second polarizing cube beam splitter before entering a microscope objective (Nikon, 100x, N.A. 1.4, oil immersion). This way, two optical traps of perpendicular linear polarization arise in the sample plane and the mobile trap can be laterally separated from the fixed trap with nanometer precision. The laser light passes through the sample and is collimated by a second objective (Olympus, 63x, N.A. 1.2, water immersion). A glan polarizer cube rejects the large majority of the light arising from the mobile beam. Force is deduced from the position of the bead in the fixed trap using back-focal plane interferometry [12, 13]. When a measurement cycle is completed, the molecular linkage between the two beads is broken and force is calibrated by recording the power spectral density of the bead in the fixed trap [13]. Unavoidable depolarization in the microscope objectives leads to some interference between the fixed and mobile beams, which generates parasitic force signal at small distance between the traps. The imposed frequency shift between the two laser beams avoids this parasitic signal [14]. We performed the experiments in a room of controlled temperature of 26°C. In the sample, the temperature is raised to about 33°C due to local heating by the trapping laser by a measured amount of ΔT=7°C [11].

B. Preparation of the molecular constructs

All four duplexes contain 4050 base pairs and exhibit the same nucleotide sequence, corresponding to the sequence of a portion of the *E. coli* chromosome (strain K-12, substr. MG1655), starting at the first nucleotide of the *rrlB* gene (coding for 23S rRNA), encompassing the full gene sequences of *rrlB* and *rrfB* (coding for 5S rRNA) and ending in the middle of the *murB* gene. Preparation of the four different duplexes being related, we first describe the RNA-DNA case and then consider the other three duplexes.

The DNA sequence of interest is amplified by PCR from a plasmid (gift of K. Nierhaus) containing the full *E. coli* rrnB operon sequence. PCR primers were designed in order to introduce a T7 RNA polymerase promoter sequence followed by an AflII restriction site at one extremity of the PCR product, and a FseI restriction site at the other extremity. Part of the PCR product is *in vitro* transcribed using T7 RNAP, and the RNA product is conserved. AflII digestion of the rest of the PCR product followed by Klenow treatment in the presence of biotin-dATP allows to incorporate two biotin moieties close to the 3' end of one strand. FseI digestion and ligation of a biotin-modified DNA oligonucleotide adds three biotins close to the 5' end of the same strand.

The goal of the next step (strand-exchange step) is to replace the unmodified DNA strand by the *in vitro* transcribed RNA. For this purpose, DNA and RNA are first denatured at high temperature and the resulting ss-strands are incubated together in temperature and solvent conditions that strongly favor RNA/DNA heteroduplex over dsDNA duplex formation [11, 15]. Subsequently, residual dsDNA duplexes are digested with EcoRI (to avoid any interference in the force experiments). Finally an RNA oligonucleotide, with two biotin modifications is ligated to the RNA 3' end of the heteroduplex.

The DNA-RNA duplex is prepared similarly. PCR primers are designed to act on opposite plasmid strands compared to the RNA-DNA case. Oligonucleotides and ligations are adapted such that the RNA strand carries biotins close to both ends, while the DNA strand exhibits biotins close to its 3' end only. Preparation of the dsDNA construct follows the protocol used for the RNA-DNA construct until the strand-exchange step. The latter is not required for dsDNA (and of course the EcoRI restriction step is omitted); the final dsDNA construct is obtained by ligating a DNA oligonucleotide carrying two biotin modifications. For the dsRNA construct, two PCRs and two *in vitro* transcriptions are performed to prepare two complementary RNA strands. The RNA strand intended to be biotinylated at each extremity (5' and 3') is *in vitro* transcribed in presence of GMP in large excess over GTP, i.e. to obtain a majority of RNA molecules with a single phosphate group at their 5' extremity, thus ready to be ligated to the adequate oligonucleotide. Biotinylation of this RNA strand is performed using a DNA-splint ligation procedure and ligating biotinylated RNA oligonucleotides with T4 RNA ligase 2 [16]. The two RNA strands are then hybridized and the biotin groups at the 3' extremity of the so far non-modified RNA strand are introduced using the same procedure than for the RNA-DNA duplex.

III. RESULTS

Four different double-stranded nucleic acid constructs have been prepared as described in the Materials and Methods section. They all contain exactly the same nucleotide sequence, except for the obvious T to U replacement when going from DNA to RNA (the sequence is described in the Materials and Methods section). Multiple biotin modifications were introduced at three of the four extremities of these duplexes and used for specific attachment to two streptavidin-coated beads. The beads are captured with two optical traps: the position of one optical trap is kept fixed to measure force by back focal plane interferometry, while the other trap is displaced with constant velocity to repeatedly strain and relax the investigated construct. This experimental configuration is schematically represented in Fig.1

A. The four duplexes at a common condition of salt and velocity

Below about 25 pN, the force-displacement curves of the four constructs exhibit rises of increasing slope, which remain identical upon relaxation (Fig.2). This part of each curve corresponds to a regime of entropic polymer elasticity at low forces, followed by a regime of enthalpic elasticity at intermediate forces. It is well described by the extensible worm-like chain model [19]. The curvature of the force-displacement curves changes sign around 25 pN. This softening has been observed for dsDNA before and has been attributed to twist-stretch coupling [4]. For all four duplexes the force-displacement relations measured below the overstretching plateau are well described by the twistable worm-like chain model, a theoretical description that takes twist-stretch coupling into account in terms of two phenomenological parameters (see SI). The force levels F_p

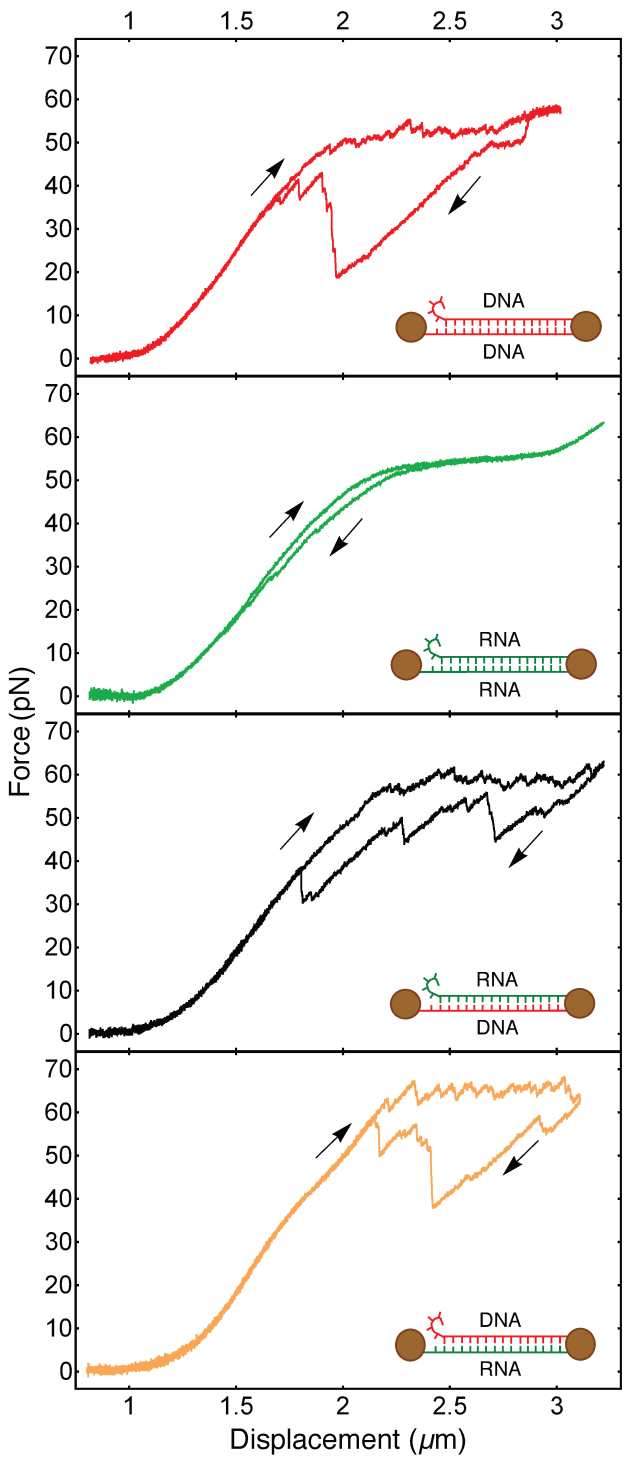

FIG. 2: Measured force-displacement curves of the four types of nucleic acid duplexes. From top to bottom, dsDNA, dsRNA, RNA/DNA hybrid and DNA/RNA hybrid are shown. Arrows indicate the direction of imposed displacement; a curve measured upon pulling and the curve measured upon subsequent retraction is shown in each case. The molecular duplexes and their three-point attachements to the two beads are schematically represented in the insets. Every duplex exhibits one 5' extremity that is free to peel off. The four measurements have been performed under same buffer condition (100 mM KCl, 5 mM $MgCl_2$, 20 mM Hepes, pH 7.6) and at same displacement velocity (100 nm/s).

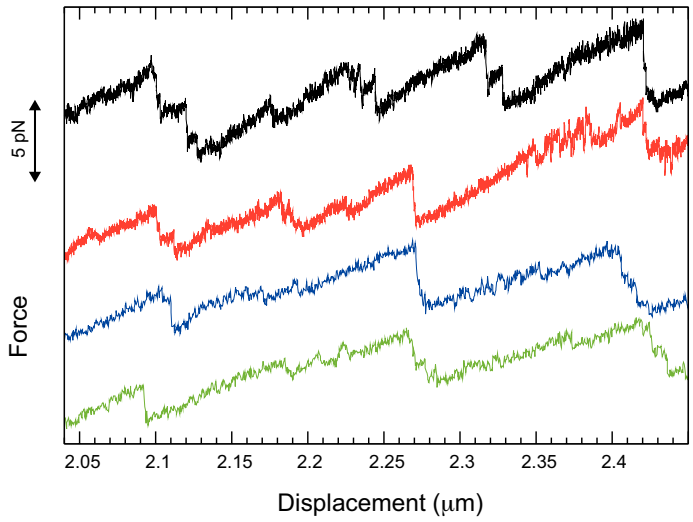

FIG. 3: Detailed view of four force-displacement curves measured on the overstretching plateau of the RNA-DNA hybrid. The lowest two curves correspond to two consecutive measurements of the same molecule and the two upper curves to two other molecules. The curves are shifted vertically for better visibility of the details. For the two lower curves, we used the buffer conditions and displacement velocity of Fig.2, while the two upper curves were measured with smaller displacement velocity (10 nm/s) and higher monovalent salt (400 mM KCl, 5 mM $MgCl_2$, 20 mM Hepes, pH 7.6).

(about 1.8 pN standard deviation of the measured values) of the overstretching plateaus are close, but for the present case of equivalent base-sequence, same buffer and same displacement velocity we nevertheless can resolve a distinct order,

$$F_p^{DNA/RNA} \simeq 64.8 \text{ pN} > F_p^{RNA/DNA} \simeq 60.0 \text{ pN} > F_p^{dsDNA} \simeq 57.6 \text{ pN} > F_p^{dsRNA} \simeq 55.2 \text{ pN}.$$

Surprisingly strong qualitative differences are observed between the overstretching curves of the dsRNA duplex on the one hand and the overstretching curves of the other three duplexes on the other hand. For dsRNA, the plateau is smooth and exhibits rather small hysteresis, whereas for the other three duplexes, the overstretching signal reveals a succession of sawtooth-shaped peaks and a strong hysteresis with deep decreases in force followed by sudden returns. In Fig.3 we present a zoom into the overstretching plateau measured upon stretching the RNA-DNA hybrid. The curves display successions of sawtooth-shaped peaks. Typically, a phase of slow increase in force is followed by a sudden force reduction. The same characteristic features are observed on the overstretching plateaus of the dsDNA and DNA-RNA constructs. The figure also shows that details of the sawtooth-shaped force signals can be similar from one pulling cycle to another and from one molecule to another.

B. Effects of salt concentrations and displacement velocity

It was shown that overstretching of dsDNA can involve different mechanisms and that the prevalence of one or another of these mechanisms depends on salt conditions and displacement velocity [8, 9]. Under the experimental conditions of Fig.2, we observe both sawtooth-like and smooth overstretching for dsDNA. A smooth region appears for instance at a displacement of about

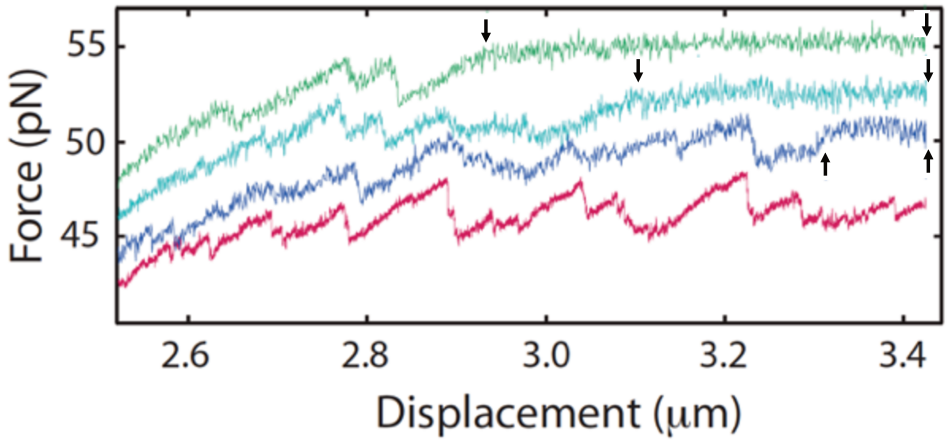

FIG. 4: Effect of the displacement velocity on the force signal recorded during overstretching an RNA-DNA hybrid. The represented force-displacement curves correspond to four successive pulling sequences applied to the same molecule. The displacement velocities are 10 nm/s (red), 300 nm/s (blue), 500 nm/s (cyan) and 750 nm/s (green). Blue, cyan and green curves are shifted by 2, 4 and 6 pN, for better visualization. Regions between arrows exhibit a smooth force signal. The fraction of the curves occupied by smooth parts increases with increasing displacement velocity. Buffer used in the measurements of this figure: 150 mM NaCl, 10 mM $MgCl_2$, 10 mM Hepes, pH 7.6.

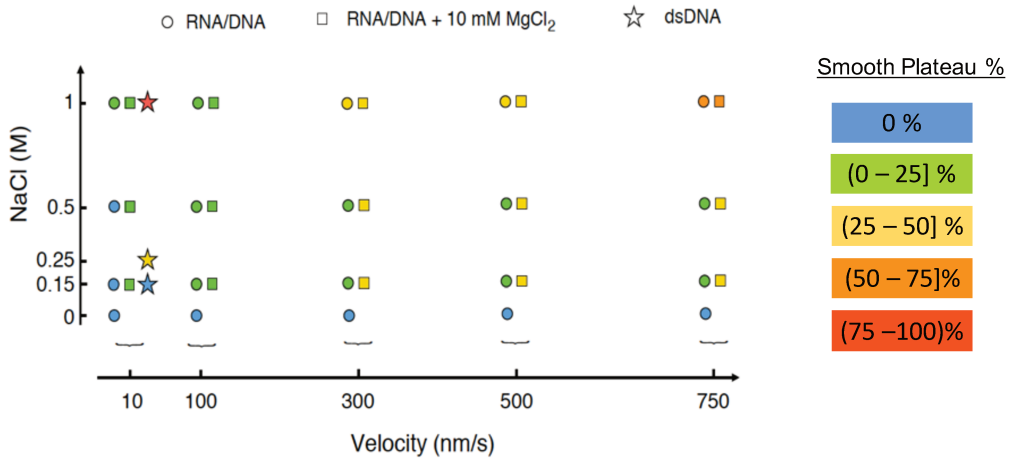

FIG. 5: Influence of NaCl concentration (vertical axis) and velocity (horizontal axis) on the overstretching plateau of RNA-DNA hybrids. The percentage of smooth plateau is marked by a color code as given at the right of the figure. For pulling velocities up to 500 nm/s, the percentage of smooth plateau remains less than 50% whatever the NaCl or $MgCl_2$ concentration, whereas for 750 nm/s smooth plateau becomes dominant at the highest NaCl concentration used (1M), both in the absence (circles) or presence (squares) of 10 mM $MgCl_2$. The data for dsDNA (stars) were taken from [8].

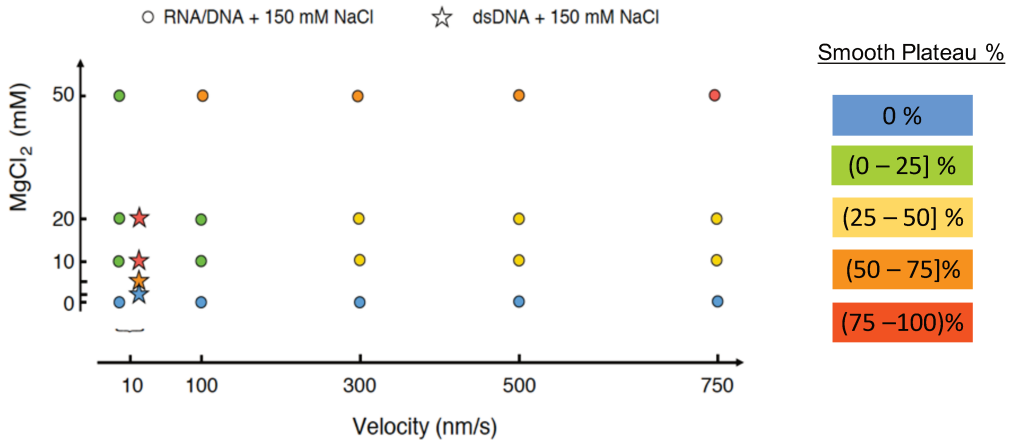

FIG. 6: Influence of $MgCl_2$ concentration (vertical axis) and velocity (horizontal axis) on the overstretching plateau of RNA-DNA hybrids at 150 mM NaCl (circles). The percentage of smooth plateau is marked by a color code as given at the right of the figure. At 100 nm/s, the percentage of smooth overstretching plateau is negligible at 10 mM $MgCl_2$, but it increases to 50-75 % at 50 mM $MgCl_2$. An increase in velocity to 750 nm/s leads to 25-50 % smooth plateau already at 10 mM $MgCl_2$, whereas at 50 mM the conversion to smooth overstretching plateau is virtually complete. The data for dsDNA (stars) were taken from [8].

3 μm in the top panel of Fig.2. This observation indicates coexistence of peeling (responsible for sawtooth-like pattern) and at least one other mechanism (associated with a smooth signal). In Fig.4, we present force versus displacement curves measured on the RNA-DNA hybrid at various displacement velocities. The percentage of the smooth signal increases with increasing velocity. In Figs. 5 and 6, our data on salt and velocity dependence of this percentage is summarized. Fig.5 shows the percentage for velocities ranging from 10 nm/s to 750 nm/s and NaCl concentrations ranging from 0 to 1M, while Fig.6 shows the percentage for NaCl concentration of 150 mM, various velocities and $MgCl_2$ concentrations between 0 and 50 mM. Divalent salt has a much stronger effect than monovalent salt. The parameter window for which peeling occurs is much wider for the RNA-DNA hybrid than for dsDNA. Roughly speaking, the higher the velocity or salt concentration, the higher the percentage of smooth region. Qualitatively the same trends have been previously reported for dsDNA [8].

C. Theoretical description of overstretching by peeling and bubble formation

As described before [8, 9], depending on experimental conditions, dsNA can overstretch via three different mechanisms: peeling, melting bubble formation and transition into an S-conformation (see Fig.1). As the transition and the energy of initial and final states are rather well known for peeling and melting bubble formation, here we will introduce a theoretical description for these two overstretching mechanisms.

TABLE 1: Experimental and theoretical overstretching forces, together with energy and length values of the theoretical description.

	F_p (pN)	F_{the} (pN)	E_b (k_BT/bp)	E_{ss} (k_BT/nt)	E_{ds} (k_BT/bp)	Δl (nm/nt)
dsDNA	57.6 ± 1.8	57.7	2.30	1.84	1.20	0.208
dsRNA	55.2 ± 1.8	55.5	3.33	1.01	0.56	0.239
RNA/DNA	60.0 ± 1.8	60.1	2.38	1.21	0.43	0.274
DNA/RNA	64.8 ± 1.8	63.9	2.38	1.08	0.74	0.217

Experimental plateau values F_p are obtained by averaging 20-50 measured overstretching plateaus for each duplex type. All these measurements were performed under the experimental conditions of Fig.2. The calculated forces F_{the} verify $E(F_{the}) = 0$, where $E(F)$ is defined by Eq.1. The binding energies E_b are taken from the literature [20–22]. The elastic energies E_{ss} and E_{ds} and the length difference $\Delta l = l_{ss} - l_{ds}$ are evaluated at force F_{the}.

1. Overstretching by peeling

The force-induced peeling phenomenon can be described by a conversion of a double stranded nucleic acid into two single strands, only one of which stays under tension. This transition implies rupture of hydrogen bonds, modified stacking interactions as well as changes in elastic energy. We consider the free-energy difference $E(F)$ between a state $(n+1)$ exhibiting $n+1$ peeled base pairs and a state (n) with n peeled base pairs at constant force F. The construct would peel progressively for $E(F) < 0$, reanneal progressively for $E(F) > 0$, and the states (n) and $(n+1)$ would have equal probability for $E(F) = 0$.

$$E(F) = E_b + E_{ss} - E_{ds} - F\,(l_{ss} - l_{ds}) \tag{1}$$

E_b is an average energy required to open one base pair, which we obtained from published unified nearest-neighbour ΔG^0_{37} parameters (see Table 1 and SI). For simplicity, we call this parameter "base pair binding energy" in this paper. E_{ss} denotes the energy per nucleotide required to stretch a single-stranded nucleic acid (ssNA) from zero-force to a force F and E_{ds} is the energy per base pair required to stretch a double-stranded nucleic acid (dsNA) from zero to F. The term $F\,(l_{ss} - l_{ds})$ describes the mechanical work (length change times force) , where l_{ss} and l_{ds} are the length per nucleotide of a ssNA stretched to force F and the length per base pair of a dsNA stretched to force F, respectively. We derived E_{ss}, E_{ds}, l_{ss} and l_{ds} from force measurements on ssDNA and dsDNA. A detailed description of the model and its parameters is presented in SI.

Equation (1) allows us to obtain a phase diagram, predicting the dsNA $\rightarrow$ ssNA transition (Fig.7). It consists of two different regions: a region where the considered molecule has preference for a double stranded conformation ($E > 0$) and a region where it has preference for a single-stranded conformation ($E < 0$). Zero-energy defines the predicted force level of the overstretching plateau. At $F = 0$, the energy E is simply given by E_b. Below about 2 pN, the energy versus force curves $E(F)$ exhibit an initial increase with force, which is explained by a negative $(l_{ss} - l_{ds})$. At higher force, $(l_{ss} - l_{ds})$ becomes positive, leading to a monotonic decrease of $E(F)$. Largely depending on its starting level E_b, the curve either penetrates (dsDNA, RNA-DNA, DNA-RNA) or stays well above (dsRNA) the peeling region. Finally, approaching a critical force F_{max}, the

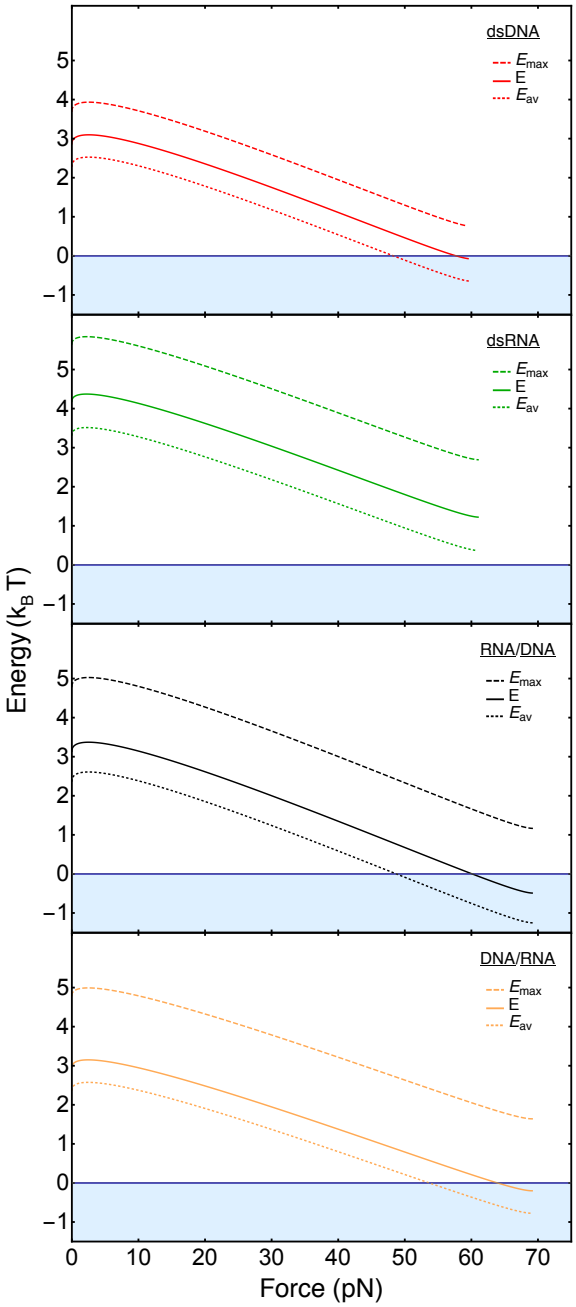

FIG. 7: Energy difference $E(F)$ for overstretching by peeling, calculated using Eq.1. Energy versus force curves are presented for dsDNA (red), dsRNA (green), RNA-DNA (black) and DNA-RNA (orange). The energy diagram is divided into two regions: a region where the molecules are double-stranded (white) and a region where the peeled state is energetically favorable (light blue). For calculating the dotted lines, we used the literature binding energies E_b=$E_{av}(F = 0)$ (Table 1). E_{max} is the free energy of the strongest base pair, E_{av} is the average free energy of all base pairs. For calculating the solid lines, we enhanced E_b by small amounts that are 41 %, 37 %, 32 % and 24 % of the difference between E_{max} and E_b (from top to bottom). $E = E_{av} + E_{add}$. These enhancements are introduced in order to phenomenologically account for sequence heterogeneity and out-of-equilibrium effects (see SI, section II. 2. E_{add} term). They lead to agreement between measured and theoretically predicted plateau forces for the three cases where peeling is observed. When the applied force reaches the threshold value for which the energy E is zero, dsDNA, RNA-DNA and DNA-RNA hybrids start to peel, whereas dsRNA always remains far away from the peeling region.

curves show slight positive curvature before stopping. The positive curvature is caused by the twist-stretch coupling term. At this point the molecule under tension completely unwinds (no twist is left) and the theoretical description of the twist-stretch coupling loses its physical meaning at forces above F_{max} (see SI). Application of the described model to our experimental data gives two major results, (i) peeling is predicted only for three of the four molecular constructs and the significantly higher value of E_b is the main reason why peeling is not predicted for dsRNA.

2. Overstretching by melting bubble formation

Overstretching by melting bubble formation involves rupture of dsNA base pairs; the mechanism is similar to peeling in this respect. As a difference, however, melting bubble formation results in single strands that both remain under tension, while one strand relaxes in the peeling case. The applied force F is distributed among the two strands, either equally if the two strands are of the same nature ($F_1 = F_2 = F/2$; for dsDNA and dsRNA), or unequally if the two strands are of different nature ($F_{DNA} \neq F_{RNA}$; $F_{DNA} + F_{RNA} = F$; for RNA-DNA and DNA-RNA). The process can be described by equation 1 as for peeling, albeit the following modifications in the elastic energies of the single strands and the mechanical work.

$$E(F) = E_b + E^*_{ss} - E_{ds} - F\,(l^*_{ss} - l_{ds}) \tag{2}$$

where

$$E^*_{ss} = \begin{cases} 2E^{DNA}_{ss}(F/2) & \text{for dsDNA} \\ 2E^{RNA}_{ss}(F/2) & \text{for dsRNA} \\ E^{DNA}_{ss}(F_{DNA}) + E^{RNA}_{ss}(F_{RNA}) & \text{for DNA-RNA and RNA-DNA} \end{cases}$$

$$l^*_{ss} = \begin{cases} l^{DNA}_{ss}(F/2) & \text{for dsDNA} \\ l^{RNA}_{ss}(F/2) & \text{for dsRNA} \\ l^{DNA}_{ss}(F_{DNA}) = l^{RNA}_{ss}(F_{RNA}) & \text{for DNA-RNA and RNA-DNA} \end{cases}$$

Using equation 2 we constructed an equivalent to the peeling case phase diagram (Fig.8), again with two regions. In the lower region ($E < 0$) the molecule has a preference to form melting bubbles along its NA chain. Zero energy indicates equilibrium between double stranded and melting bubble conformations. The energy versus force curves look alike to the peeling case, with a start value of E_b and a round maximum around 5 pN that is followed by a continuous decrease. The free energy versus force curves reach their end before the $E = 0$ phase boundary, which indicates that overstretching via melting bubble formation is energetically non-favorable for all four duplexes. For more details see SI.

IV. DISCUSSION

A. Force levels of overstretching by peeling

Under the conditions of section II.A, the dsDNA, DNA-RNA and RNA-DNA constructs show sawtooth-like force signals and pronounced hysteresis. These observations are clear signatures of peeling. We present in Table 1 the average values of the force plateaus F_p measured with increasing displacement, and the calculated forces F_{the} for overstretching by peeling. We observe differences of a few pN between the plateau forces of the three constructs. Within the experimental

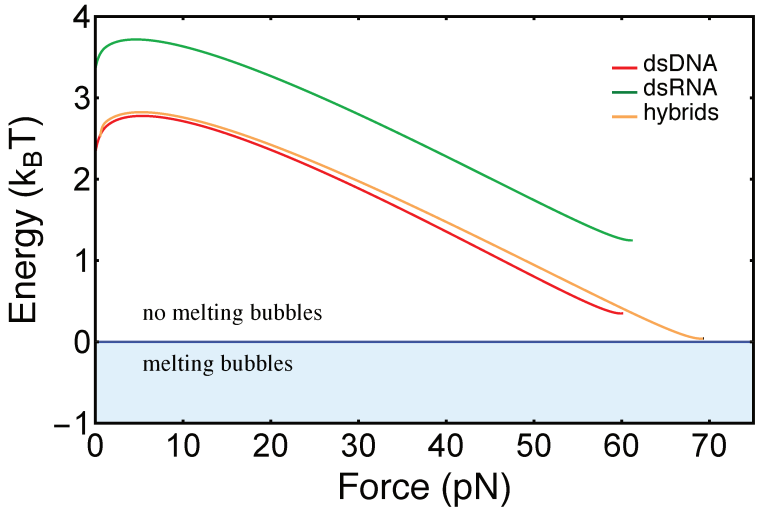

FIG. 8: Energy difference $E(F)$ for overstretching by melting bubble formation, calculated using Eq.2. Energy versus force curves are presented for dsDNA (red), dsRNA (green) and the two hybrids (RNA-DNA and DNA-RNA, orange). The energy diagram is divided into two regions: a region where the molecules are entirely double-stranded (white) and a region where a state containing melting bubbles is energetically favorable (light blue). Melting bubble formation is predicted for none of the duplexes.

uncertainty, which is mainly due to variations in size, shape and refractive index of the beads, the measured forces F_p agree with the calculated forces F_{the}. The differences between the plateau forces of the three constructs can be explained by inspecting Fig.7 and the energy and length values presented in Table 1. Comparing first dsDNA and RNA-DNA, we see that the two energy-force relations are very similar, except for a small relative shift in the vertical direction. This indicates that the higher binding energy E_b is responsible for the higher plateau force of RNA-DNA as compared to dsDNA. Comparing then RNA-DNA and DNA-RNA, the binding energies are equal by symmetry, but different relative extension $\Delta l = l_{ss} - l_{ds}$ leads to a smaller slope of the energy versus force curve and in turn a higher plateau force for DNA-RNA. Since the double-strand lengths l_{ds} of DNA-RNA and RNA-DNA are equal by symmetry, we find that the different lengths of the single-strands under tension ($l_{ss}^{DNA} > l_{ss}^{RNA}$) cause the observed difference in plateau force.

B. Sequence-dependent force signal observed for peeling

Peeling is a sequence-dependent overstretching mechanism. In this work, we use a three-point-attachment that was previously described by Gross et al [4] and for which peeling always involves the same single strand. The peeling front thus propagates in a one-dimensional manner through the base sequence, which explains that details of the force signals measured at increasing displacement can be similar (Fig.3). In this situation, the theoretical description of the sequence-dependent force signals is related to the description of NA unzipping [3, 4, 23]. Sequence regions exhibiting high (low) GC content lead to high (low) force. Molecular stick-slip dynamics induces sawtooth-like features in the force-displacement curves. Typically, the peeling front advances little in front of a

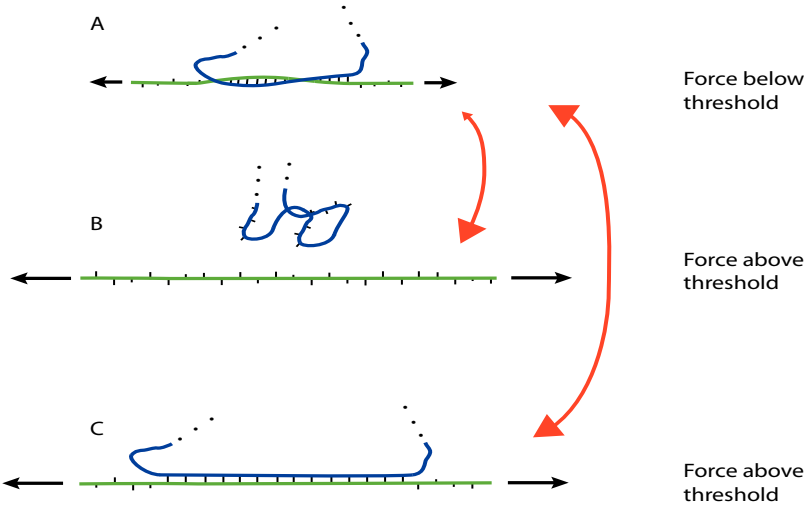

FIG. 9: Schematic representation of the implications of different force-induced overstretching modes. In panel A a single-strand (green) is submitted to a pulling force below the overstretching threshold (short black arrows). This strand is hybridized with a complementary base sequence (blue) forming a local duplex structure. When force increases above the overstretching threshold (long black arrows) there are two possibilites. Overstretching might occur by peeling and/or bubble-formation and the hybridized motif unbinds (panel B). Alternatively, S-structure formation might occur and the hybridized structure remains bound (panel C). As explained in the text, the transition from A to B is widely irreversible when the force redecreases below threshold, while the transition from A to C is reversible. This is illustrated by asymmetric and symmetric red double-arrows, respectively.

sequence with increasing GC content. During this 'stick' phase force rises slowly. Subsequently a 'slip' event occurs once the local energy barrier is overcome. Then the peeling front advances rapidly and the force drops. The energy landscape is determined by the base sequence, but the exact positions where the transitions occur exhibit stochastic variation. Flipping between discrete states is sometimes observed (for instance on the right part of the red curve), which is a signature of close-to-equilibrium dynamics. Sawtooth-shaped peaks and force flips are observed for the RNA-DNA, the dsDNA and the DNA-RNA constructs and these qualitative features agree with the observations of Gross et al [4], who studied a three-point-attachment dsDNA construct containing a pKYB1 sequence of 8393 base pairs.

C. RNA-DNA overstretching depends on displacement velocity and salt

Earlier studies showed that overstretching of dsDNA can be due to different mechanisms, leading to a complex phase diagram that depends on salt conditions, displacement velocity, sequence and topology [4, 8–10]. In particular, it was shown that at high ionic strength S-DNA formation is favored over peeling in topologically open DNA [8]. In this case, Zhang et al observed peeling and S-DNA formation, but not bubble formation [9]. The present work indicates that the overstretching phase diagram of an RNA-DNA heteroduplex is of similar complexity and qualitatively ressembles the one of dsDNA. In both cases, peeling dominates at low salt and velocity, while

overstretching with a smooth force signal occurs more frequently at high salt concentrations and high displacement velocities. However, we observe quantitative differences that are illustrated in Figs.4-6. Peeling remains the dominant overstretching mechanism for a much wider range of salt concentrations and displacement velocity in the RNA-DNA hybrid than in the dsDNA construct. We attribute the observed smooth overstretching to S-NA formation, because bubble formation is predicted to be energetically non-favorable (Fig.8). For the peeling mechanism, the calculated differences between the energies of RNA-DNA and dsDNA are small and the dsDNA energy lies slightly below the one of the RNA/DNA hybrid (Fig.7). The observation that RNA-DNA peeling dominates over a wider parameter space therefore suggests that the energy of the heteroduplex S-phase is higher than the one of the dsDNA S-phase. We do not know the reason for this difference and whether it is of structural or dynamical origin. Regarding structural difference, the RNA-DNA heteroduplex forms an A-type double-helix, which is more compact than the B-type DNA double helix [24]. As an example for different dynamical properties, some of us have shown previously that unfolding and refolding of hairpin structures under force occur faster and significantly closer to equilibrium in DNA than in RNA [25].

D. Peeling and bubble-formation do not occur in dsRNA

We observe remarkable qualitative differences between the force curves for overstretching dsRNA as compared to the curves for overstretching the other duplexes. They are illustrated in Fig.2: smooth plateau and weak hysteresis occur for dsRNA, while dsDNA, RNA-DNA and DNA-RNA show rapidly varying force-signals and pronounced hysteresis. We investigated a wide range of conditions, monovalent salt from 10 to 100 mM, divalent salt from 0 to 5 mM and displacement velocities from 10 to 100 nm/s, but for dsRNA we did not observe the characteristic signatures of peeling. Smooth plateaus were also observed in an earlier study, where dsRNA molecules were overstretched with a velocity of 500 nm/s in 150 mM, 300 mM and 500 mM NaCl [26]. Our theoretical description predicts absence of peeling for dsRNA and indicates that this absence is caused by the higher base pair binding energy ($E_b = 3.33$ k_BT) of dsRNA as compared to dsDNA and the heteroduplexes (2.30 and 2.38 k_BT, respectively). As described in SI section II.A.1, this interpretation holds for a wide range of salt concentrations, including close-to-physiological salt condition. Bubble formation could explain smooth overstretching, but the results presented in Fig.8 suggest that it is not energetically favorable. We note that the remaining mechanism, the transition from an A-type helix to S-conformation, does not expose local single-stranded sequences of the RNA molecule. Biological implications of this result are discussed in the following subsection.

E. RNA overstretches without generating single strands: biological relevance

To what extent does the absence of single-strand generation attributed to our data on dsRNA help an RNA molecule achieve its biological role? Does this property match the functions of RNA, which differ from the ones of DNA?

Forces above 50 pN occur in the biological cell [27]. For instance, the maximum force the mitotic spindle exerts on a single moving chromosome in anaphase amounts to 700 pN. This force was measured *in vivo* [28]. During assembly of many viruses, a powerful molecular motor compacts the genome into a preassembled capsid. Forces of up to 100 pN were measured for bacteriophage ϕ29 DNA packaging *in vitro* [29, 30]. To the best of our knowledge, to date there exists neither a published report about an *in vivo* measurement of forces acting on RNA structures

nor one about a force measurement on viral RNA packaging. Unzipping of RNA double helices requires forces of 10-20 pN, depending on their base sequence [2, 25, 31, 32]. This mechanical opening and closing of RNA duplexes frequently occur close to thermal equilibrium; the opening fork breathes thermally, manifesting itself by flips in the observed signal. This equilibrium implies that formation of an RNA duplex from complementary strands generates forces of 10-20 pN. In view of the complex structures adopted by RNA, including numerous helices, tertiary structure interactions and sometimes also interactions with RNA-binding proteins, we think that major conformational transitions are susceptible to generate transient forces that exceed the overstretching threshold at critical positions within an RNA structure.

To make overstretching relevant *in vivo*, it is also necessary that the force acts on a duplex in shear mode. When a single strand is hybridized with a short complementary NA sequence, peeling can occur and/or bubbles can form, as illustrated in Fig.1. When the force acting on the former strand exceeds the threshold for overstretching, the complementary strand is susceptible to dissociate and diffuse away. This is illustrated schematically in Fig.9, where it corresponds to the transition from panel A to panel B.

From the preceding two paragraphs, we are thus left with the idea that force-induced generation of single-strands could occur from both the force magnitude and topology points of view. What would this possibility imply for RNA? The implications are schematically represented in Fig.9. If RNA duplexes were prone to peeling or bubble formation, when F increases above the overstretching threshold, dissociation of the complementary RNA strand would occur. This would happen even if high force is reached only for a short moment. The two single-strands would separate, move and engage binding with other RNA residues (or proteins), thus leading to either an irreversible or a long-lasting change of RNA structure, detrimental to its normal cellular activity. An asymmetric double arrow between panels A and B represents the irreversible behaviour. In contrast, if overstretching occurs via a mechanism that preserves base pairing, like the S-RNA formation that we attribute to our experimental observations, the initial RNA structure resumes readily when force falls below the overstretching threshold (symmetric double arrow between panels A and C). This general idea is further illustrated in SI section III, where we consider RNA action within the protein-synthesis machinery.

ACKNOWLEDGEMENTS

We are grateful to Marc Dreyfus for critical reading of the manuscript. This work has been supported by the Human Frontier Science Program [RGP008/2014].

[1] Essevaz-Roulet B, Bockelmann U, Heslot F (1997) Mechanical separation of the complementary strands of DNA. Proc. Natl. Acad. Sci. USA 94: 11935-11940.

[2] Liphardt J, Onoa B, Smith SB, Tinocco I, Bustamante C (2001) Reversible unfolding of single RNA molecules by mechanical force. Science 292: 733-737.

[3] Bockelmann U, Thomen P. Essevaz-Roulet B, Viasnoff V, Helot F (2002) Unzipping DNA with optical tweezers: high sequence sensitivity and force flips. Biophys J 82: 1537-1553.

[4] Gross P, Laurens N, Oddershede LB, Bockelmann U, Peterman EJG, Wuite GJL (2011) Quantifying how DNA stretches, melts and changes twist under tension. Nature Physics 7: 731-736.

[5] Cluzel P, Lebrun A, Heller C, Lavery R, Viovy JL, Chatenay D, Caron F (1996) DNA: an extensible molecule. Science 271: 792-794.

[6] Smith S B, Cui Y, Bustamante C (1996) Overstretching B-DNA: the elastic response of individual double-stranded and single-stranded DNA molecules. Science 271: 795-799.

[7] Bustamante C, Smith S B, Liphardt J, Smith D (2000) Single-molecule studies of DNA mechanics. Curr. Opin. Struct. Biol. 10: 279-285.

[8] King GA, Gross P, Bockelmann U, Modesti M, Wuite GJL, Peterman EJG (2013) Revealing the competition between peeled ssDNA, melting bubbles and S-DNA during DNA overstretching using fluorescence microscopy. Proc. Natl. Acad. Sci. USA 110: 3859-3864.

[9] Zhang X, Chen H, Le S, Rouzina I, Doyle P S, Yan J (2013) Revealing the competition between peeled ssDNA, melting bubbles, and S-DNA during DNA overstretching by single-molecule calorimetry. Proc. Natl. Acad. Sci. USA 110:3865-3870.

[10] Paik DH, Perkins TT (2011) Overstreching DNA at 65 pN does not require peeling from free ends or nicks. J. Am. Chem. Soc. 133: 3219-3221.

[11] Geffroy L, Mangeol P, Bizebard T, Bockelmann U (2017) RNA unzipping and force measurements with a dual optical trap. Methods Mol. Biol. 1665: 25-41.

[12] Gittes F, Schmidt C F (1998) Interference model for back-focal-plane displacement detection in optical tweezers. Opt. Lett. 23: 7-9.

[13] Neuman K, Block S M (2004) Optical trapping. Rev. Sci. Instrum. 75: 2787-2809.

[14] Mangeol P, Bockelmann U (2008) Interference and crosstalk in double optical tweezers using a single laser source. Rev. Sci. Instrum 79: 083103.

[15] Dean M (1987) Determining the hybridization temperature for Si nuclease mapping. Nucleic Acids Res. 15: 6754.

[16] Vilfan I D, Kamping W, van den Hout M, Candelli A, Hage S, Dekker N H (2007) An RNA toolbox for single-molecule force spectroscopy studies. Nucleic Acids Res. 35: 6625-6639.

[17] Fu H, Chen H, Zhang X, Qu Y, Marko J F, Yan J (2010) Transition dynamics and selection of the distinct S-DNA and strand unpeeling modes of double helix overstretching. Nucleic Acids Res. 39: 3473-3481.

[18] Arias-Gonzalez J R (2014) Single-molecule portrait of DNA and RNA double helices. Integr. Biol. 6: 904-925.

[19] Odijk T (1995) Stiff chains and filaments under tension. Macromolecules 28: 7016-7018.

[20] Xia T, SantaLucia Jr J, Burkard M E, Kierzek R, Schroeder S J, Jiao X, Cox C, Turner D H (1998) Thermodynamic parameters for an expanded nearest-neighbor model for formation of RNA duplexes with Watson-Crick base pairs. Biochemistry 37: 14719-735.

[21] SantaLucia Jr J (1998) A unified view of polymer, dumbbell, and oligonucleotide DNA nearest-neighbor thermodynamics. Proc. Natl. Acad. Sci. USA 95: 1460-65.

[22] Sugimoto N, Nakano S, Katoh M, Matsumura A, Nakamuta H, Ohmichi T, Yoneyama M, Sasaki M (1995) Thermodynamic parameters to predict stability of RNA/DNA hybrid duplexes. Biochemistry 34: 11211-216.

[23] Bockelmann U, Essevaz-Roulet B, Heslot F (1998) DNA strand separation studied by single molecule force measurements. Phys. Rev. E 58: 2386-2394.

[24] Marin-Gonzalez A, Vilhena J G, Perez R, Moreno-Herrero F (2017) Understanding the mechanical response of double-stranded DNA and RNA under constant stretching forces using all-atom molecular dynamics. Proc. Natl. Acad. Sci. USA 114: 7049-7054.

[25] Bercy M, Bockelmann U (2015) Hairpins under tension: RNA versus DNA. Nucleic Acids Res. 43: 9928-9936.

[26] Herrero-Galán E H, Fuentes-Perez M E, Carrasco C, Valpuesta J M, Carrascosa J L, Moreno-Herrero F, Arias-Gonzalez J R (2012) Mechanical identities of RNA and DNA double helices unveiled at the single-molecule level. J. Am. Chem. Soc. 135: 122-131.

[27] Roca-Cusachs P, Conte V, Trepat X (2017) Quantifying forces in cell biology. Nat. Cell Biol. 19: 742-751.

[28] Nicklas R B (1983) Measurements of the force produced by the mitotic spindle in anaphase. J. Cell Biol. 97: 542-548.

[29] Smith D E, Tans S J, Smith S B, Grimes S, Anderson D L, Bustamante C (2001) The bacteriophage ϕ29 portal motor can package DNA against a large internal force. Nature 413: 748-752.

[30] Rickgauer J P, Fuller D N, Grimes S., Jardine P J, Anderson D L, Smith D E (2008) Portal motor velocity and internal force resisting viral DNA packaging in bacteriophage ϕ29. Biophys. J. 94: 159-167.

[31] Harlepp S, Marchal T, Robert J, Léger J-F, Xayaphoummine A, Isambert H, Chatenay D (2003) Probing complex RNA structures by mechanical force. Eur. Phys. J. E 12: 605-615.

[32] Mangeol P, Bizebard T, Chiaruttini C, Dreyfus M, Springer M, Bockelmann U (2011) Probing ribosomal protein-RNA interactions with an external force. Proc. Natl. Acad. Sci. 108: 18272-18276.

[33] Kaczanowska M, Rydén-Aulin M (2007) Ribosome biogenesis and the translation process in *Escherichia coli*. Microbiol. Mol. Biol. Rev. 71: 477-494.

[34] Lorsch J R (2002) RNA chaperones exist and DEAD box proteins get a life. Cell 109: 797-800.

[35] Wen J-D, Lancaster L, Hodges C, Zeri A-C, Yoshimura S H, Noller H F, Bustamante C, Tinocco Jr I (2008) Following translation by single ribosomes one codon at a time. Nature 452: 598-603.

[36] Liu T, Kaplan A, Alexander L, Yan S, Wen J-D, Lancaster L, Wickersham C E, Fredrick K, Noller H, Tinoco Jr I, Bustamante C J (2014) Direct measurement of the mechanical work during translocation by the ribosome. eLife 3: e03406.

[37] Schuwirth B S, Borovinskaya M A, Hau C W, Zhang W, Vila-Sanjurjo A, Holton J M, Cate J H D (2005) Structures of the bacterial ribosome at 3.5 Å resolution. Science 310: 827834.

Overstretching double-stranded RNA, double-stranded DNA and RNA-DNA duplexes – Supplementary Information –

L. Melkonyan[1], M. Bercy[1], T. Bizebard[2], and U. Bockelmann[1]
1 Nanobiophysique, ESPCI Paris
10 rue Vauquelin, 75005 Paris, France

2 Expression Génétique Microbienne,
IBPC, CNRS UMR 8261
13 rue Pierre et Marie Curie,
75005 Paris, France

I. FITTING THE MEASURED FORCE-EXTENSION RELATIONS

In figure S1, we present average values and mean-square deviations of measured force-displacement curves for the four different constructs. The part below the overstretching plateau is fitted to the twistable worm-like chain model. The fit function is shown as a blue solid line. It relates the imposed displacement to the measured force F. The displacement equals the sum of the length x of the molecule and the shifts F/k_{trap} of the beads compared to their equilibrium positions in the optical traps. The length of the molecule x is the product of the number of base pairs N_b ($N_b = 4050$ for our constructs) and the length per base pair l_{ds}. The latter is given by the analytical expression [1, 2]

$$l_{ds}(F) = L_c^{ds}\left(1 - 1/2\sqrt{\frac{k_B T}{F L_p}} + \frac{F}{K - g(F)^2/C}\right), \tag{1}$$

where L_c^{ds}, L_p and K are respectively the crystallographic length per base pair, the persistence length and the stretch modulus per base pair of the nucleic acid (NA) duplex. The twist-stretch coupling is parametrized by the twist rigidity C and the function $g(F)$. The latter is described by

$$g(F) = \begin{cases} g_0 + g_1 F_c & \text{for} \quad F \leq F_c \\ g_0 + g_1 F & \text{for} \quad F > F_c \end{cases}, \tag{2}$$

with three parameters, g_0, g_1 and F_c. The parameters used to describe the average force-extension relations are presented in Table S1.

Although we measured a significant number of force-displacement relations for each of the four NA duplexes, the experimental data do not allow determining the seven parameters in a unique way. The parameter set shown in Table S1 is consistent with the information available from the literature. Our lengths L_c^{ds} and L_p agree with published values for dsDNA and dsRNA [3–7]. The parameters K, C, g_0, g_1 and F_c affect the shape of the force-extension curve at high force. For the twist rigidity C of all duplexes, we take a value reported in the literature for dsDNA [1, 8]. Moreover we assume a common critical force F_c that is close to the value published for dsDNA [1]. Our parameter set displays the reported opposite sign of the twist-stretch-coupling value $g_0 - g_1 F_c$

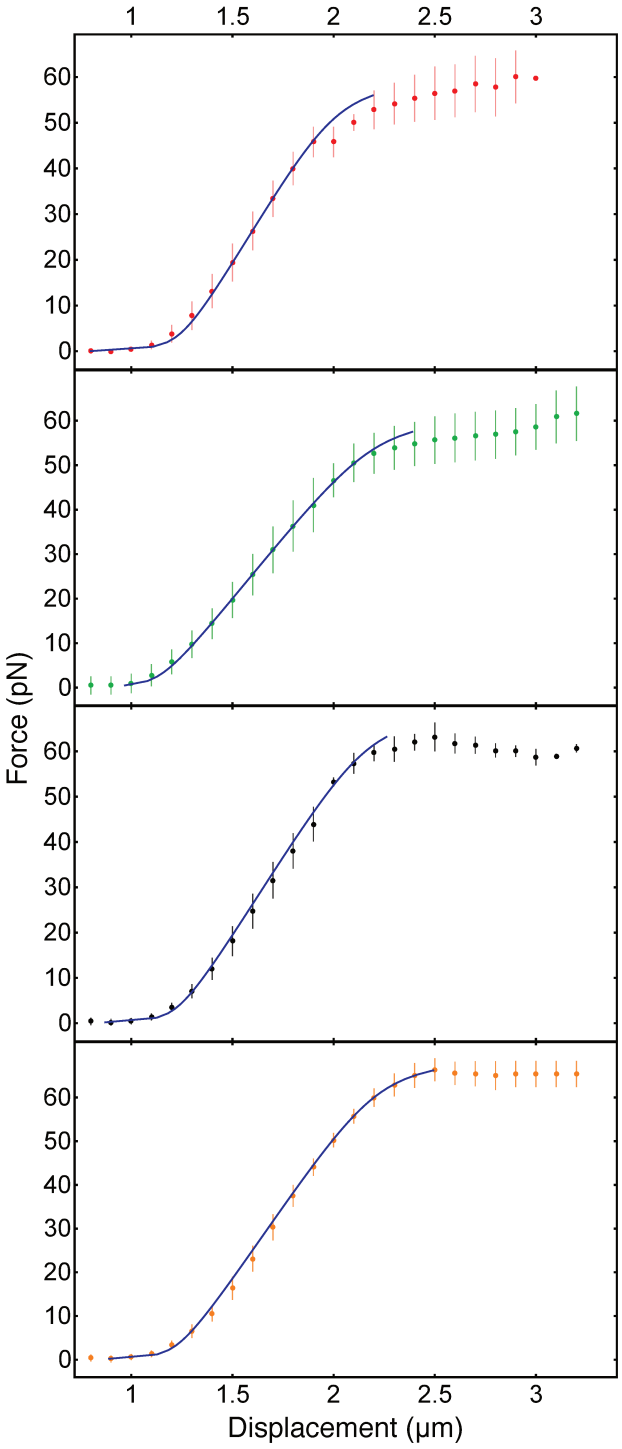

FIG. S1: Average force-displacement curves of the four different molecular duplexes. Data for dsDNA, dsRNA, RNA-DNA and DNA-RNA are presented from top to bottom and are based on 76, 92, 57 and 24 individual measurements, respectively. Dots and vertical bars show average force and mean-square deviation. Solid blue lines represent fits to a twistable worm-like chain model. In all measurements used for this figure we used the buffer condition and displacement velocity given in the caption of main text Fig.2.

TABLE S1: Parameters used to describe the measured average force-extension relations.

	L_c^{ds} (nm)	L_p (nm)	K (pN)	C (pN nm^2)	g_0 (pN nm)	g_1 (nm)	F_c (pN)
dsDNA	0.310	50	1074	440	-530	19.5	25
dsRNA	0.290	63	870	440	-520	23.4	25
RNA/DNA	0.312	55	948	440	-525	20.85	25
DNA/RNA	0.313	55	870	440	-525	19.2	25

for dsDNA as compared to dsRNA [9–13]. We did not find corresponding literature information for hetero-duplexes.

II. THEORETICAL DESCRIPTION OF OVERSTRETCHING

A. Peeling

The force-induced peeling phenomenon can be described by a conversion of a double stranded nucleic acid into two single strands, only one of which stays under tension. This transition implies rupture of hydrogen bonds, modified stacking interactions as well as a change in elastic energy of the molecular construct. In free energy terms this process will have the following representation:

$$E(F) = E_b + E_{add} + E_{ss} - E_{ds} - F\left(l_{ss} - l_{ds}\right) \tag{3}$$

Let us consider each energy term separately.

1. E_b term

The base pair binding energies E_b are phenomenological free energies for opening a base pair of the duplex. As such, they contain both enthalpic and entropic contributions and are sequence-dependent. Neglecting sequence heterogeneity and assuming a GC-content of 50 % (the average GC-content of our constructs is 52 %), we simply use an arithmetic average of the ΔG^0_{37} values reported for the different base pairs in the nearest-neighbor models of the literature. For 1M monovalent salt and no divalent salt, we thus obtain $E_b = 2.30$ for dsDNA from SantaLucia [14], $E_b = 3.33$ for dsRNA from Xia et al [15] and $E_b = 2.38$ for the heteroduplex from Sugimoto et al [16], with energies expressed in units of k_BT at room-temperature (300K).

The variation of E_b with monovalent salt concentration was estimated using the DNA formula available from the literature [14]. We find that all E_b values decrease by about 0.6 k_BT when the salt concentration decreases from 1M to 150 mM. A rough estimate of the variation with divalent salt was also performed, using the approach proposed by Qi et al [17]. We thus find an increase by about 0.8 k_BT when the salt cconditions change from 150 mM monovalent salt to 150 mM monovalent salt plus 50 mM divalent salt. For the sake of simplicity, we use the E_b values corresponding to 1M monovalent salt and no divalent salt for all calculations presented in this paper.

2. E_{add} term

We add a positive correction E_{add} to phenomenologically account for sequence heterogeneity and out-of-equilibrium effects that are both neglected in our theoretical description.

Sequence heterogeneity causes a rough energy landscape, while the simple theoretical description assumes a smooth landscape. In the former case, the peeling front will perform a biased random walk through the base sequence, experiencing a rapidly varying potential. From the physics point of view, the process encountered in peeling NA sequences is thus similar to the one encountered in DNA unzipping, the latter being discussed in the literature. The fundamental differences between unzipping heterogeneous and homogeneous base sequences were described [18], the amplitude of the thermal "breathing" of the opening fork was shown to decrease with increasing local stiffness [19] and it was predicted that the advancement of the opening fork in a heterogeneous sequence is given by the times required to overcome the maxima of the energy landscape [20]. We also note that peeling experimentally does not occur at thermal equilibrium. Peeling is expected to occur above the theoretically predicted equilibrium force when trap distance increases, while re-annealing is expected to occur below the theoretical equilibrium force. The resulting difference between the average peeling and re-annealing forces is clearly apparent in our measurements with dsDNA, DNA-RNA and RNA-DNA (see main text Fig.2). This hysteresis was reported before for dsDNA [1]. We note that sequence heterogeneity and out-of-equilibrium effects are expected to increase the peeling force as compared to our theoretical description.

As it is difficult to explicitely include sequence heterogeneity and out-of-equilibrium effects, we take them into account in a phenomenological way, by adding a positive energy E_{add}. This way, it is possible to align the theoretical prediction with the measured force of the overstretching plateau for all three cases of experimentally observed overstretching by peeling (main text, Fig.7 and Table 1). This agreement is achieved with E_{add} values that are small compared to the average binding energies E_b. The E_{add} values (0.57, 0.86, 0.76 and 0.58 k_BT for dsDNA, dsRNA, RNA/DNA and DNA/RNA, respectively) amount to only 24-41% of the difference between the binding energies of the most stable basepairs and the average binding energies. Whether or not E_{add} is introduced, the experimentally observed order of the average forces of the peeling-plateaus agrees with the theoretical prediction.

3. E_{ss} term

E_{ss} denotes the energy per nucleotide required to stretch a single-stranded nucleic acid (ssNA) from zero-force to a force F. We theoretically describe the elasticity of the ssNA by the worm-like chain model [2],

$$l_{ss}(F) = L_c^{ss}\left(1 - 1/2\sqrt{\frac{k_BT}{FL_p}}\right). \tag{4}$$

We use $L_c^{ss} = 0.70$ nm and $L_c^{ss} = 0.65$ nm for the crystallographic length per nucleotide of ssDNA and ssRNA, respectively. The persistence lengths are $L_p = 1.20$ nm for ssDNA and $L_p = 1.37$ nm for ssRNA. These values were obtained by fitting force-displacement measurements of DNA and RNA hairpin structures [21, 22]. Integration of Eq.4 leads to the energy E_{ss},

$$E_{ss}(F) = F\, l_{ss}(F) - \int_0^F l_{ss}(f)\, df = \frac{L_c^{ss}}{2}\sqrt{\frac{k_BT}{L_p}}F.$$

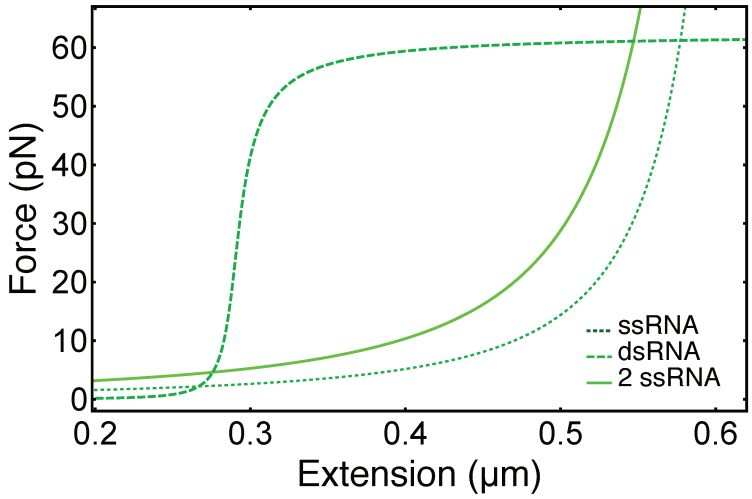

FIG. S2: Comparison of theoretical force-extension relations of dsRNA (dashed), ssRNA (dotted) and two parallel non-interacting ssRNA strands (solid).

4. E_{ds} term

E_{ds} is the energy per base pair required to stretch a double-stranded nucleic acid (dsNA) from zero-force to a force F. It is obtained by analytical integration of the force-displacement relation $l_{ds}(F)$ of Eq.1, using

$$E_{ds}(F) = F\, l_{ds}(F) - \int_0^F l_{ds}(f)\, df.$$

The simple theoretical description of twist-stretch coupling according to Eq.1 and 2 exhibits an unphysical divergence. Approaching a critical force $F = \left(\sqrt{C\,K} - g_0\right)/g_1$ from below, the predicted dsNA length goes to infinity. This softening also causes a divergence of E_{ds}. To avoid using the model outside its validity range, we restrict our calculation to forces below a threshold value. The threshold is given by the force for which the dsNA length becomes equal to the length of two parallel non-interacting ssNA strands. The curves presented in main text figures 7 and 8 are restricted to the corresponding force ranges. For illustration, the theoretical length of dsRNA is compared to the length of two parallel non-interacting ssRNA strands in Fig.S2.

5. $F\ (l_{ss} - l_{ds})$ term

The length of the molecular construct under tension changes when a base pair opens, since a dsNA fragment of one base pair under force F is then converted to an ssNA nucleotide under force F. The corresponding mechanical work $W = F\ (l_{ss} - l_{ds})$ is performed by the force measuring device; a double optical trap with two beads in our case. The force-dependent lengths l_{ss} and l_{ds} are given by Eqs.1 and 4. Typically, a single-stranded NA is longer than a double-stranded NA at given force, with the notable exception of the low-force entropic regime. In Fig.S2, we present theoretical force-extension relations of ssRNA, dsRNA and two parallel strands of non-interacting

ssRNA molecules.

B. Melting bubble formation

Overstretching by melting bubble formation involves rupture of dsNA base pairs; the mechanism is similar to peeling in this respect. As a difference, however, melting bubble formation results in single strands that both remain under tension, while one strand relaxes in the peeling case. The applied force F is distributed among the two strands, either equally if the two strands are of the same nature ($F_1 = F_2 = F/2$; for dsDNA and dsRNA), or unequally if the two strands are of different nature ($F_{DNA} \neq F_{RNA}$; $F_{DNA} + F_{RNA} = F$; for RNA-DNA and DNA-RNA). The process is described in main text section III.C.2. Here we complement the description by one detail. It regards how the couple $\{F_{DNA}, F_{RNA}\}$, occuring in the heteroduplex case of main text Eq.2, can be calculated. For given F, we numerically determine F_{DNA} as the zero of the function

$$y(F_{DNA}) = l_{ss}^{DNA}(F_{DNA}) - l_{ss}^{RNA}(F - F_{DNA}),$$

where $l_{ss}^{DNA}(F)$ and $l_{ss}^{RNA}(F)$ are given by Eq.4. F_{RNA} is obtained afterwards by calculating $F_{RNA} = F - F_{DNA}$.

III. THE RIBOSOME AS AN ILLUSTRATION

Translation of messenger RNA (mRNA) into protein is achieved by the ribosome. The ribosome is a nucleoprotein particle, made of ribosomal RNA (rRNA) and ribosomal proteins (r-proteins), with mass proportions of roughly 2/3 rRNA and 1/3 r-protein in bacteria. Assembly of the ribosome involves a complex series of processes, where the folding of rRNA is accompanied by r-proteins and external protein components [23]. While there are other RNA-mediated processes of relevance for the present discussion, like RNA splicing, regulation of transcription and translation, exportation of preribosomes through nuclear pores, we choose ribosome assembly and processive translation to specifically illustrate the idea of main text subsection IV.E.

A. Ribosome assembly

The *E.coli* ribosome contains three rRNA molecules. The longest one is the 23S rRNA of the large subunit with 2904 nucleotides. Due to very easy complementary base pairing and the additional possibility to form non-Watson-Crick interactions, an RNA as large as the 23S rRNA exhibits a daunting number of possible structures and folding into the native structure is highly complex [24]. Alternate secondary or tertiary structures form kinetic traps of long lifetime and it is known that r-proteins and non-ribosomal proteins (folding helpers) assist ribosome assembly *in vivo*. This implies that structure, energy landscape and folding pathways of the rRNA molecules would be particularly sensitive to the local mechanical denaturation discussed in the previous subsection. Ribosome assembly is highly cooperative, involves folding of large RNA domains with many RNA-RNA and RNA-protein interactions and therefore can generate high forces. We thus tentatively suggest that overstretching without single-strand exposure is essential for the choreography of ribosome assembly.

B. Processive translation

The ribosome also develops forces during processive translation. Single-molecule measurements directly showed that the *E. coli* ribosome is able to mechanically open hairpin structures in the mRNA and to develop a force of 13 pN during translation [25, 26]. This force is too small to induce overstretching. Development of significantly higher force could be detrimental to the regulation of translation by secondary structure in mRNA, as pointed out by the authors [26]. Structural studies showed that the ribosome structure rearranges during processive translation. Swiveling of the head of the small subunit and a ratchet-like relative motion of the two subunits were observed; RNA bridges between the two subunits do rearrange, or even break [27]. It is therefore conceivable that some of the corresponding forces exceed the threshold of dsRNA overstretching and that overstretching without single-strand generation could prevent the ribosome from damaging itself during the translation elongation cycle.

---

[1] Gross P, Laurens N, Oddershede LB, Bockelmann U, Peterman EJG, Wuite GJL (2011) Quantifying how DNA stretches, melts and changes twist under tension. Nature Physics 7: 731-736.

[2] Odijk T (1995) Stiff chains and filaments under tension. Macromolecules 28: 7016-18.

[3] Herrero-Galán E H, Fuentes-Perez M E, Carrasco C, Valpuesta J M, Carrascosa J L, Moreno-Herrero F, Arias-Gonzalez J R (2012) Mechanical identities of RNA and DNA double helices unveiled at the single-molecule level. J. Am. Chem. Soc. 135: 122-131.

[4] Saenger W (1984) Principles of Nucleic Acid Structures. Springer, New York.

[5] Abels J A, Moreno-Herrero F, van der Heijden T, Dekker C, Dekker N H (2005) Single-Molecule Measurements of the Persistence Length of Double-Stranded RNA. Biophys. J. 88: 2737-2744.

[6] Baumann C G, Smith S B, Bloomfield V A, Bustamante C (1997) Ionic effects on the elasticity of single DNA molecules. Proc. Natl. Acad. Sci. USA 94: 6185-6190.

[7] Hagermann P J (1997) Flexibility of RNA. Annu. Rev. Biophys. Biomol. Struct. 26: 139-156.

[8] Bryant Z, Stone M D, Gore J, Smith S B, Cozzarelli R, Bustamante C (2003) Structural transitions and elasticity from torque measurements on DNA. Nature 424: 338-341.

[9] Marin-Gonzalez A, Vilhena J G, Perez R, Moreno-Herrero F (2017) Understanding the mechanical response of double-stranded DNA and RNA under constant stretching forces using all-atom molecular dynamics. Proc. Natl. Acad. Sci. USA 114: 7049-7054.

[10] Gore J et al (2006) DNA overwinds when stretched. Nature 442: 836-839.

[11] Lionnet T, Joubaud S, Lavery R, Bensimon D, Croquette V (2006) Wringing out DNA. Phys. Rev. Lett 96: 178102.

[12] Lipfert J et al (2014) Double-stranded RNA under force and torque: similarities to and striking differences from double-stranded DNA. Proc. Natl. Acad. Sci. USA 111: 15408-15413.

[13] Liebl K, Drsata T, Lankas F, Lipfert J, Zacharias M (2015) Explaining the striking difference in twist-stretch coupling between DNA and RNA: a comparative molecular dynamics analysis. Nucleic Acids Res. 43: 10143-10156.

[14] SantaLucia Jr J (1998) A unified view of polymer, dumbbell, and oligonucleotide DNA nearest-neighbor thermodynamics. Proc. Natl. Acad. Sci. USA 95: 1460-65.

[15] Xia T, SantaLucia Jr J, Burkard M E, Kierzek R, Schroeder S J, Jiao X, Cox C, Turner D H (1998) Thermodynamic parameters for an expanded nearest-neighbor model for formation of RNA duplexes with Watson-Crick base pairs. Biochemistry 37: 14719-735.

[16] Sugimoto N, Nakano S, Katoh M, Matsumura A, Nakamuta H, Ohmichi T, Yoneyama M, Sasaki M (1995) Thermodynamic parameters to predict stability of RNA/DNA hybrid duplexes. Biochemistry 34: 11211-216.

[17] Qi Z, Pugh R A, Spies M, Chemla Y R (2013) Sequence-dependent base pair stepping dynamics in XPD helicase unwinding. eLife 2: e00334.

[18] Lubensky D K, Nelson D R (2002) Single molecule statistics and the polynucleotide unzipping transition. Phys. Rev. E 65: 031917.

[19] Bockelmann U, Thomen P. Essevaz-Roulet B, Viasnoff V, Helot F (2002) Unzipping DNA with optical tweezers: high sequence sensitivity and force flips. Biophys J 82: 1537-1553.

[20] Bockelmann U, Viasnoff V (2008) Theoretical study of sequence dependent nanopore unzipping of DNA. Biophys. J. 94, 2716-2724.

[21] Bercy M, Bockelmann U (2015) Hairpins under tension: RNA versus DNA. Nucleic Acids Res. 43: 9928-9936.

[22] Bercy M (2015) Les structures secondaires dans l'ARN : une étude par mesure de force sur molécules uniques. PhD manuscript (unpublished).

[23] Kaczanowska M, Rydén-Aulin (2007) Ribosome biogenesis and the translation process in *Escherichia coli*. Microbiol. Mol. Biol. Rev. 71: 477-494.

[24] Lorsch J R (2002) RNA chaperones exist and DEAD box proteins get a life. Cell 109: 797-800.

[25] Wen J-D, Lancaster L, Hodges C, Zeri A-C, Yoshimura S H, Noller H F, Bustamante C, Tinocco Jr I (2008) Following translation by single ribosomes one codon at a time. Nature 452: 598-603.

[26] Liu T, Kaplan A, Alexander L, Yan S, Wen J-D, Lancaster L, Wickersham C E, Fredrick K, Noller H, Tinoco Jr I, Bustamante C J (2014) Direct measurement of the mechanical work during translocation by the ribosome. eLife 3: e03406.

[27] Schuwirth B S, Borovinskaya M A, Hau C W, Zhang W, Vila-Sanjurjo A, Holton J M, Cate J H D (2005) Structures of the bacterial ribosome at 3.5 Å resolution. Science 310: 827834.

Chapter II

Early steps of ribosome assembly

The ribosome is a ribonucleoprotein, which is the central unit of protein synthesis in the cell, and which is well conserved during evolution. Being the currently best characterized one, the ribosome of *E.coli* was chosen for this study. The 70S ribosome in *E.coli* consists of two subunits: a small subunit (30S) and a large subunit (50S). The small subunit is composed of one RNA molecule (16S rRNA) and 21 proteins and the large subunit is composed of two RNA molecules (23S and 5S rRNAs) and 33 proteins. In this work we study the assembly of the large subunit. *In vivo* the assembly of this subunit starts shortly after the beginning of the synthesis of 23S rRNA, and is completed in approximately two minutes at 37°C [13]. Already during their synthesis, the rRNAs fold and are structurally modified by ribosomal proteins. The latter are consecutively incorporated into rRNA, forming first intermediate precursors, and finally a mature and functional 50S nucleoprotein particle.

In vitro this reconstitution takes much longer, and special buffer and temperature conditions are required [14, 15, 16]. It is achieved in two steps. First, the fully transcribed 23S, 5S rRNAs and 33 ribosomal proteins are incubated in 4mM Mg^{2+} (magnesium acetate), 400mM NH_4Cl, 0.2mM EDTA, 5mM 2-mercaptoethanol for 20min at 44°C, and then, in 20mM Mg^{2+} (magnesium acetate), 400mM NH_4Cl, 0.2mM EDTA, 5mM 2-mercaptoethanol for 90min at 55°C. In the first step the 50S subunit goes though two intermediate states $RI_{50}(1)$ and $RI^*_{50}(1)$[15]. In these two states the ribonucleoprotein particle has the same composition, but a different sedimentation rate: 33S for $RI_{50}(1)$ and 41S for $RI^*_{50}(1)$. This difference reveals that the ribonucleoprotein undergoes conformational changes to pass from the intermediate $RI_{50}(1)$ to the intermediate $RI^*_{50}(1)$. The 23S rRNA and the five ribosomal proteins, namely uL4, uL24, uL22, uL13 and bL20, called "early binders", play essential roles in these conformational changes already at early stages of ribosome assembly [6, 17, 18]. These proteins consist of a globular domain located on a ribosome surface and extensions or a loop penetrating into the core of 23S rRNA and co-folding with it [19, 20, 21, 22, 23], this way stabilizing the tertiary structure of the rRNA. A fully active ribosomal particle is obtained much faster *in vivo* than *in vitro*.There are two possible explanations. First, *in vivo* the ribosomal proteins are incorporated into rRNA co-transcriptionally [24, 25], whereas *in vitro* the fully transcribed, folded 23S rRNA is incubated with proteins in an

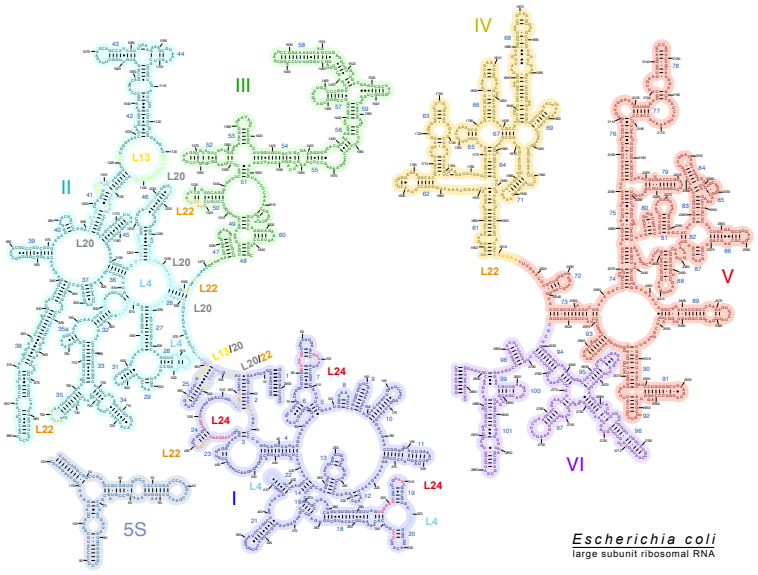

Contacts of early assembly r-proteins with 23SrRNA.
uL4: 319-324; 583-591; 608-620; 657-660; 670-676; 798-801; 1200-1205; 1244-1248; 1254-1258
uL13: 527-529; 536-539; 549; 556-559; 1005-1008; 1012; 1021-1022; 1131-1143; 2639-2643; 2767-2769
bL20: 18-19; 29-30; 513-516; 531-536; 554; 559-564; 578-583; 991-998; 1009-1012; 1150-1157; 1197-1200; 1215-1219; 1225-1227; 1247-1253;
uL22: 23-26; 485-489; 517-520; 746-751; 1260-1262; 1265-1266; 1321-1326; 2009-2014;
uL24: 81-86; 98-101, 296-302; 308-11; 335-337; 477-484, 497-501

Figure II.1: The large subunit ribosomal RNA of Escherichia Coli. The numbers indicate the position of nucleotides counting from the beginning of 5' extremity of 23S rRNA. Numbers in blue indicate the common binding sites for the proteins bL20 and uL4. The numbers in red indicate the common binding sites for the proteins bL20 and uL13.

appropriate buffer. Second, *in vivo* there are assembly helpers (RNA helicases, chaperons, maturation factors and GTPases) [26, 27, 28, 29] that help the rRNA overcome non native structures (kinetic traps) [30, 24] that have a long lifetime, as compared to the assembly kinetics, resulting in a faster assembly process as compared to *in vitro* reconstitution.

In view of such a big difference in reconstitution time and temperature, it is interesting to develop a technique which allows us to mimic the rRNA transcription *in vitro* and study the early steps of ribosome assembly. We achieved this using molecular biology techniques and optical tweezers. To mimic rRNA transcription *in vitro*,

an RNA-DNA hybrid with three attachments [31] was prepared, as described in the chapter 1. The 5' and 3' ends of the DNA strand, and the 3' end of the RNA strand are biotin modified, allowing us to attach the molecule to two streptavidin-coated polystyrene beads. The 3' ends of the DNA and RNA strands are attached to one bead, while the 5' end of the DNA strand is attached to another bead. The 5' end of the RNA strand is left free. The two beads are then trapped into two optical traps and pulled apart. The pulling velocity is kept constant and is chosen such that it corresponds to the rRNA transcription velocity *in vivo*, which is 42 bp/s [25]. This way an increasing force is exerted on the molecule between the beads. When the molecule is extended 1.7 times its crystallographic length, the RNA strand progressively, and in a well-controlled manner, peels off the DNA strand starting from its 5' end. This way the 23S rRNA is gradually liberated mimicking its transcription *in vivo*. To study the early steps of ribosome assembly we mimicked the 23S rRNA transcription in presence of five early binders: uL4, uL24, uL22, uL13, bL20, in 1μM concentration each. These proteins were shown to be essential for conformational changes of rRNA and stabilization of its tertiary structures during the early stages of the assembly [17]. Each protein has several binding sites and contacts on the 23S rRNA. They are well known, see figure II.1. This knowledge will help us to identify which proteins are incorporated co-transcriptionally and whether these known binding sites are specific or they interact with 23S rRNA also in a non-specific manner.

The experiment is as follows: First, the beads are pulled apart and 23S rRNA strand is progressively liberated until the end of its domain 3, where the five ribosomal proteins are supposed to bind. Then, the beads are brought back to their initial position, the molecule relaxes and may, or may not, return to its initial double-strand conformation. In presence of the five early binders, we expect to see modifications in the return trace. If the ribosomal proteins are incorporated into 23S rRNA during its progressive liberation, the liberated part will fold into the ribosome's native conformation and will be stabilized, thus being unable to anneal, forming the initial double stranded hybrid. Indeed, this is the case in our measurements. Moreover, increasing the number of early binders makes this effect stronger. The results are described in detail in the article below.

Chapter III

Résumé en Français

III.1 Introduction

Ce travail vise à mieux comprendre deux problèmes importants du point de vue de la physique fondamentale et de la biologie: a) le comportement mécanique et structurel des biomolécules sous une force externe appliquée et b) les premières étapes de l'assemblage des ribosomes chez *E. coli*.

Les forces jouent des rôles importants en biologie. Elles sont exercées sur des molécules d'ADN, d'ARN et leurs hybrides par des moteurs moléculaires et des enzymes [1, 2, 3, 4, 5] au cours de nombreux processus biologiques importants : réplication de l'ADN, recombinaison homologue, réparation de brins, conditionnement, transcription, assemblage des ribosomes, translation, division cellulaire, etc. Ces forces peuvent entraîner des modifications topologiques, conformationnelles ou structurelles induisant une extension, une torsion ou une génération d'un seul brin. Ce dernier point est particulièrement important, car il peut donner lieu à des interactions parasites et la formation de structures non natives, ce qui peut en outre affecter le processus biologique impliquant des duplex composés d'ADN ou d'ARN. Par conséquent, la compréhension de la réponse mécanique de l'ADN, des duplex d'ARN et des hétéroduplex ADN-ARN (hybrides ADN-ARN) à une force appliquée présente un grand intérêt, non seulement pour la physique fondamentale, mais aussi pour la biologie. Elle permet de mieux comprendre les régulations moléculaires et cellulaires et peut même être utile pour le développement d'applications en biotechnologie et en médecine.

Plus précisément, nous nous posons les questions suivantes :

Problème 1.

Quelles sont les réponses mécaniques des acides désoxyribonucléiques (ADN), des duplex d'acide ribonucléique (ARN) et des hétéroduplex ADN-ARN aux forces externes appliquées? Quelles sont les différences entre les réponses des différents duplex moléculaires?

Problème 2.

Quel est l'effet des protéines ribosomales à liaison précoce (early-binding r-proteins) uL4, uL24, uL22, uL13, bL20 lors des premières étapes de l'assemblage des ribosomes?

Ces deux questions seront traitées dans les chapitres I et II du manuscrit en anglais,

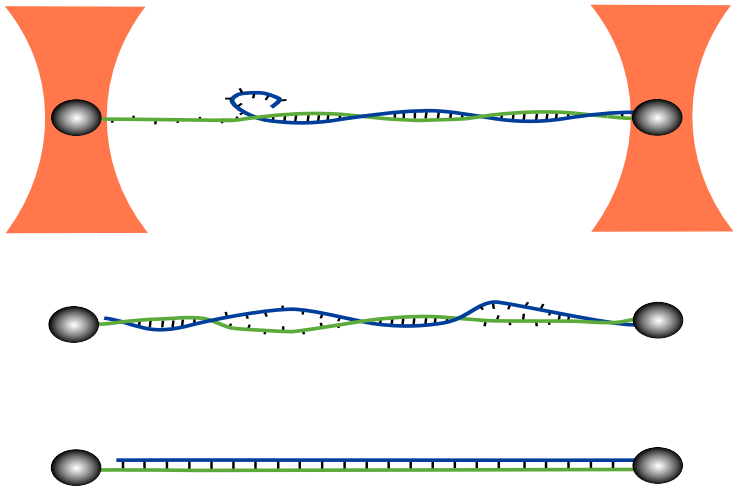

Figure III.1: Représentation schématique de la configuration de mesure et des trois mécanismes de surétirement. Le duplex d'acide nucléique est attaché par trois de ses quatre extrémités à deux billes microscopiques (les billes et la molécule ne sont pas à la même échelle). Les deux billes de chaque haltère sont capturées dans des pièges optiques séparés (orange). Les courbes force-déplacement sont obtenues en mesurant la position d'une bille dans le piège à la précision nanométrique, tandis que l'autre piège est déplacé. Le pelage du brin libre, la formation de bulles et la formation de la structure S sont présentés de haut en bas.

et repris ici en français dans les sections I et III.3. Au chapitre de la partie anglaise, nous avons présenté brièvement les objets moléculaires de l'étude, le dispositif expérimental et ensuite la manière de préparer les constructions moléculaires pour les mesures de force à molécule unique. Des protocoles détaillés sont fournis en annexe.

Considérons maintenant les deux projets élaborés dans cette thèse.

III.2 Comparaison entre quatre constructions moléculaires

Des forces agissent sur l'ADN et l'ARN dans la cellule biologique. Ils induisent une déformation élastique et une torsion, peuvent donner lieu à des transitions conformationnelles et structurelles et parfois conduisent à l'ouverture de paires de bases ainsi qu'à de profondes modifications de l'empilement de bases et des interactions tertiaires. La génération de brins simples à partir d'un duplex contenant des brins d'ADN ou d'ARN est particulièrement importante du point de vue biologique, car elle peut entraîner des interactions parasites et des structures non natives. Ces duplex sont omniprésents dans la cellule. Outre la double hélice d'ADN étant composée de deux brins simples complémentaires, la plupart des molécules d'ARN contiennent de nombreuses parties hélicoïdales et beaucoup de ces duplex locaux sont des éléments essentiels des structures d'ARN natif. De plus, des hétéro-duplex d'ADN et d'ARN sont produits

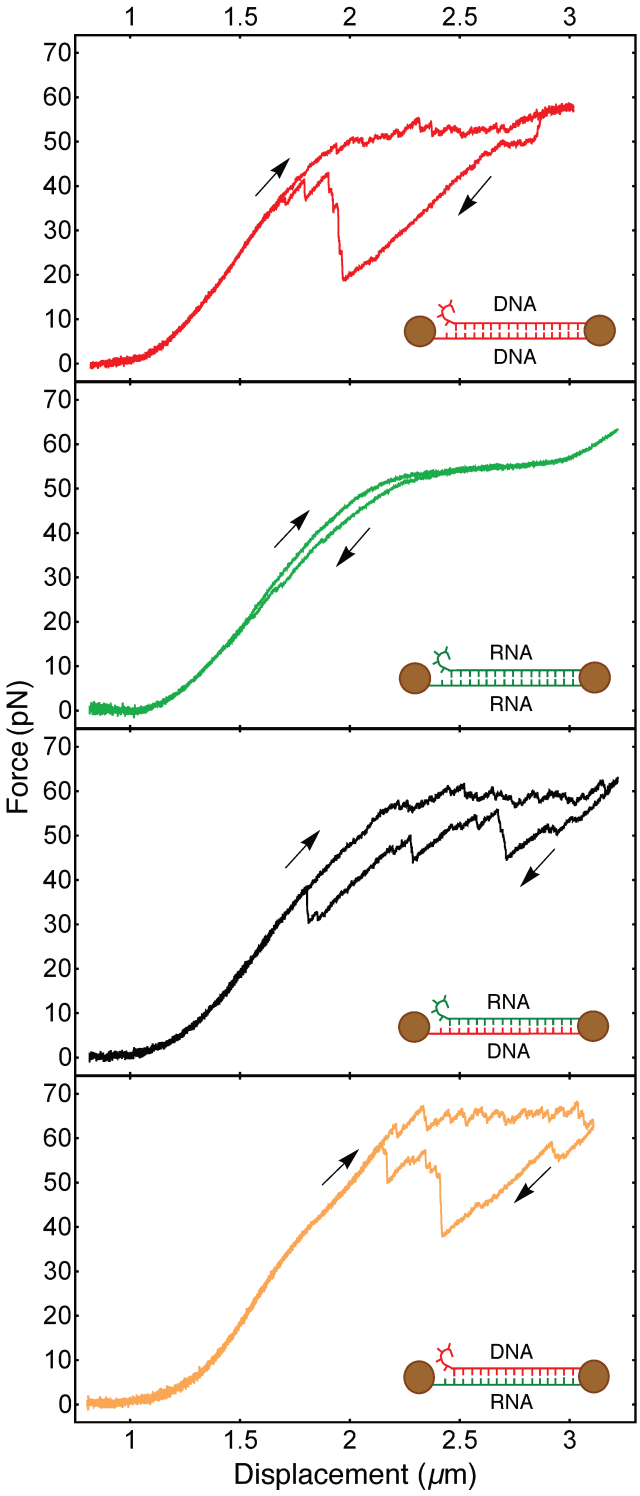

Figure III.2: Courbes de déplacement de force mesurées pour les quatre types de duplex d'acide nucléique. De haut en bas, l'ADN hybride ADNdb, ARNdb, ARN/ADN et l'ADN/ARN sont présentés. Les flèches indiquent la direction du déplacement imposé; une courbe mesurée lors de la traction et la courbe mesurée lors de la rétraction ultérieure sont indiquées dans chaque cas. Les duplex moléculaires et leurs attaches sont représentés schématiquement dans les encarts. Chaque duplex présente une extrémité 5' qui est libre de se détacher. Les quatre mesures ont été effectuées dans les mêmes conditions de tampon (100 mM KCl, 5 mM $MgCl_2$, 20 mM Hepes, pH 7.6) et à la même vitesse de déplacement (100 nm/s).

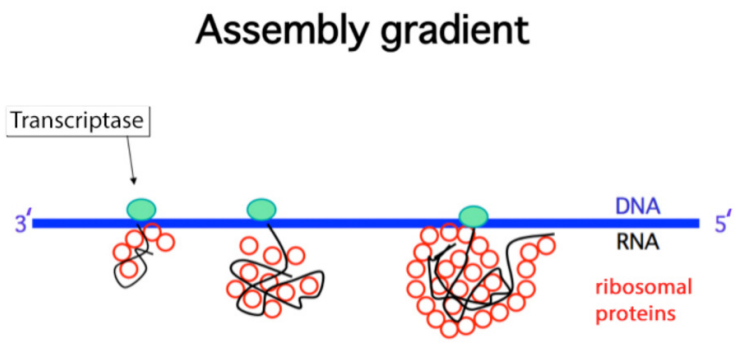

Figure III.3: L'hypothèse du "gradient d'assemblage" : les progrès de la synthèse d'ARNr définissent le progrès de l'assemblage.

dans la réplication de l'ADN, sa transcription, la régulation des gènes et les systèmes d'édition de gènes.

Des mesures à molécule unique ont montré que la force mécanique peut générer des brins uniques de différentes manières : Dans la configuration de décompression ("unzipping"), les forces tirent les deux brins au bout d'un duplex dans des directions opposées et peuvent les séparer mécaniquement. Dans la configuration de pelage, qui se produit lors de l'étirement excessif des duplex d'acide nucléique (AN), les forces agissent le long de l'axe hélicoïdal à partir d'extrémités opposées du duplex et un brin se détache dans un mode de cisaillement. Le surétirement de l'ADN a été découvert il y a environ deux décennies par des mesures de force à molécule unique. Les observations expérimentales ont déclenché de nombreuses études et discussions controversées à propos du mécanisme moléculaire sousjacent le surétirement de l'ADN. Récemment, il a été démontré expérimentalement que le surétirement de l'ADN peut être provoqué par plusieurs mécanismes, y compris le pelage, la formation de bulles ainsi qu'une transition structurelle à partir de l'hélice de forme B à une structure S-DNA. Ces mécanismes sont représentés schématiquement sur la Figure III.1.

Alors que le surétirement par la formation de bulles et par la transition vers la S-ADN montrent toutes deux des plateaux lisses dans la courbe force-extension, le pelage induit un motif caractéristique en forme de dent de scie.

Ici, nous étudions la transition de surétirement de quatre duplex d'acide nucléique différents par des mesures de force à molécule unique. Ces duplex sont ADN double brin (ADNdb), ARN double brin (ARNdb), un hétéro-duplex avec le brin d'ADN sous tension (ARN-ADN) et un hétéro-duplex avec le brin d'ARN sous tension (ADN-ARN). De manière surprénante, nous trouvons que dsRNA présente toujours un signal de surétirement lisse, une observation qui vaut pour une large gamme de conditions de sel et de vitesse de traction. En revanche, les trois autres duplex présentent des signaux prononcés en dents de scie lors du surétirement. La comparaison entre les données expérimentales et une description théorique basée sur l'hypothèse d'équilibre thermique local indique que le pelage et la formation de bulles ne se produisent pas pour les ARNdb.

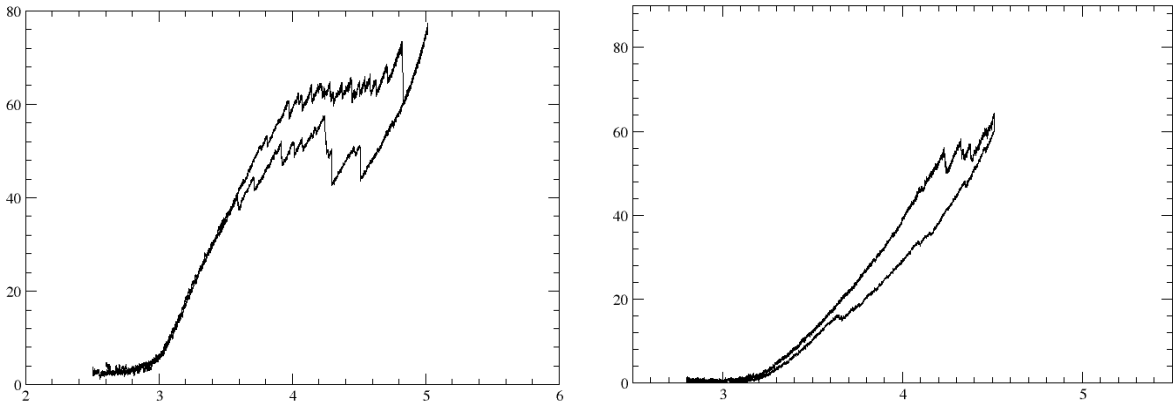

Figure III.4: Gauche: Exemple d'un cycle complet de pelage et de recuit effectué sur la construction hybride ARN-ADN sans protéines. Courbe supérieure: ouverture. Courbe inférieure: fermeture. Droite: Un cycle similaire effectué en présence des cinq *protéines de liaison précoce*. Le déplacement est arrêté après un étirement de 300 nm (donc avant celui de gauche), ce qui correspond au pelage des 1200 premiers nucléotides à l'extrémité 5' de l'ARNr 23S. Lors de la relaxation, la force mesurée diminue sans événements notables de retour soudain, contrairement à la première figure.

III.3 Influence des protines au repliement de l'ARN formant le ribosome

Cette partie de la thèse traite de l'assemblage des ribosomes; un processus important en biologie. Jusqu'à présent, la recherche sur l'assemblage a été sérieusement entravée par l'absence d'une approche *in vitro* permettant études quantitatives du repliement et de l'assemblage des ribosomes tels qu'ils se produisent *in vivo*. Nous présentons une technique innovante inspirée par les techniques utilisées dans la première partie de cette thèse. Appliquant une force sur les hétéroduplex ARN-ADN spécialement conçus, nous avons libéré de manière répétitive l'ARN, que nous avons dans la suite recuit ("re-anneal"), le tout avec un contrôle total sur la vitesse de la génération du simple brin d'ARN et de son orientation. Nous pouvons donc étudier le repliement de l'ARN au fur et à mesure de son émergence, imitant ainsi l'assemblage des ribosomes bactériens. Les protéines ribosomales se liant à l'ARNr libéré progressivement sont ensuite détectées par mesure de forces.

Pourquoi cette étude? Le ribosome est la machine moléculaire essentielle responsable pour la biosynthèse des protéines chez tous les organismes vivants. Une question clé est de comprendre les raisons de la grande différence en efficacité dans l'assemblage du ribosome *in vivo* par rapport à celui *in vitro*. Bien que la biogenèse des ribosomes *in vivo* puisse se produire efficacement à des températures d'environ 37°C en quelques minutes, la reconstruction des ribosomes *in vitro* prend beaucoup plus de temps : par exemple, les sous-unités 50S prennent 90 minutes à 50° C. Deux raisons majeures ont été avancées pour expliquer cette différence. L'une est que des facteurs non-ribosomiques

sont présents *in vivo*, qui interagissent de manière transitoire avec le ribosome naissant et facilitent son assemblage. Le second est que *in vivo* les protéines ribosomiques et les facteurs d'assemblage se lient à l'ARNr au cours de sa synthèse, accélérant ainsi considérablement le processus. Le fait que l'assemblage du ribosome se produise au site de la transcription de l'ARNr dans tous les organismes apporte un soutien à cette hypothèse.

Pour conclure, la stabilisation des structures dans l'ARNr 23S par les cinq *protéines de liaison précoce* était attendue. Notre résultat confirme cette vue classique. Notre découverte principale est que les *protéines de liaison précoce* facilitent le repliement de l'ARNr dans un test *in vitro* imitant l'assemblage co-transcriptionnel. Fait intéressant, nos expériences indiquent que la stabilisation de l'ARNr 23S par des protéines-r à liaison précoce se produit déjà pendant la transcription des domaines I et II, c'est-à-dire bien avant que l'ARN 23S entier n'ait émergé. Nos résultats appuient l'hypothèse du «gradient d'assemblage».

Appendix A

Appendix

A.1 Preparation of the beads

For optical trap experiments we used three different types of streptavidin-coated polystyrene beads. They come from different suppliers and exhibit diameters of 2.19μm, 2μm and 1.76μm, respectively. Streptavidin coating of the 2.19μm beads was performed in our lab, as described in the thesis of Mathilde Bercy [31]. The other two types of beads were commercially functionalized.

The beads with 2μm diameter (lot # 24160, Polysciences, Inc.) were diluted 10x in a **storage buffer** (10μl beads + 90μl storage buffer) composed of:

- 10mg/ml (in final volume) Polyvinylpyrrolidone (PVP, catalog # P5288, Sigma-Aldrich)
- 1μl/ml (in final volume) Tween 20 (cas # 9005-64-5, Acros Organics, Fisher-scientific)
- Polylink Wash/Storage Buffer (10mM Tris, pH 8,0 ; 0,05% BSA; 0,05% Proclin 300, lot # 583450, Polysciences, Inc.).

and were ready to be coupled with biotin modified molecular constructs.

The preparation of the beads with 1.76μm diameter (catalog # SVP-15-5, Spherotech) is as follows. The beads were first washed and then, were diluted 10x and stocked in the storage buffer described above. The washing procedure is as follows. 10μl of beads were combined with 90μ Polylink Wash/Storage Buffer and were centrifuged for 5' at 500G. The supernatant was carefully removed and 100μl of Polylink Wash/Storage Buffer was added to the pellet. The solution was then sonicated for 1' at mode "power" and was centrifuged again for 5' at 500G. This procedure was repeated three times. Once the last centrifugation step was done, 100μl of storage buffer (see above) was added to the pellet. The solution was then sonicated 15' at mode "power", and the beads were ready to be coupled with biotin modified molecular constructs. For experiments with the ribosomal proteins, the beads were passivated by polyethylene glycol coupled with biotin (mPEG-biotin, item # 139-32, Laysan Bio, Inc). The passivation details are explained in the thesis of Laurent Geffroy [32]. This passivation is efficient

for all early-binding ribosomal proteins used in our experiments (uL4, uL24, uL13, uL22, uL20C), except for bL20. For the optical-trap experiments in presence of bL20, an addition of 23S ribosomal RNA was required as described below.

A.2 Preparation of dsDNA

A.2.1 Polymerase chain reaction (PCR)

The sequence of interest (4050bp) containing the genes rrlB (coding for 23S rRNA), rrfB (coding for 5S rRNA) and 1/2 murB was amplified by polymerase chain reaction (PCR) from pT7-rrnB plasmid (gift from Knud Nierhaus). The PCR primers were designed to introduce a sequence of T7 RNA polymerase and a restriction site for AflII restriction enzyme in one extremity of the PCR product (F-MB forward primer), and a restriction site for FseI restriction enzyme in the other extremity. PCR yield and stability were improved by addition of betaine (1M final concentration) and single-stranded DNA binding protein ET-SSB (200ng final amount). For PCR, 250μl of reaction solution was prepared containing the following products:

- 12.5μl of 10μM F_MB forward primer (5'→3' TAA-TAC-GAC-TCA-CTA-TAG-GGA-GA-C-AAT-TG-C-TTA-AG-G-GTT-AAG-CGA-CTA- AGC-GTA-C, Eurogentec)
- 12.5μl of 10μM R_MB reverse primer (5'→3' C-CAC-TGA-ATT-GAG-CAG-ACC-C-GG-CCG-G-AG-AGG-ATC-GAT-CAG-ACT-AAT-CAT, Eurogentec)
- 5μl mix of 10mM each dATP, dGTP, dCTP, dTTP (catalog # N0446S, NEB)
- 2μl of pT7-RB plasmid (IBPC) with concentration of 16.3ng/μl
- 2.5μl Q5® High-Fidelity DNA Polymerase with 2000 units/ml concentration (catalog # M0491S, New England Biolabs)
- 50μl of Q5® Reaction Buffer (initial concentration 5x) to have 1x final concentration (catalog # B9027S, New England biolabs)
- 50μl of 5M Betaine solution (catalog # B0300-1VL, Sigma Aldrich)
- 4μl of ET-SSB single-stranded DNA binding protein with concentration of 500μg/ml (catalog # M2401S, New England Biolabs)
- 111.5μl of distilled water.

The reaction solution was homogenized gently with a pipet and then distributed into five 200μl PCR tubes to have 50μl solution in each. The tubes with the reaction solution were then incubated in the thermo-cycler and went through the following thermal cycle:

98° C: 30”
98° C: 10”
66° C: 30” x 30
72° C: 1’30”
72° C: 5’

After incubation the PCR product was purified using Monarch® PCR & DNA Cleanup Kit (5 μg) (catalog # T1030S).

Part of purified PCR product was conserved for in vitro RNA transcription and the other part was used to perform a restriction by FseI restriction enzyme.

A.2.2 FseI restriction

Restriction of dsDNA (PCR product) by FseI restriction enzyme (catalog # R0588S, New England Biolabs) generates a 4 nucleotide long overhang at the 3’ extremity of the leading strand, i.e. a sticky end in the dsDNA. The sticky end allows to replace the restricted parts of the leading and legging strands by two DNA oligonucleotides carrying biotin modifications. The amount recommended by New England Biolabs (NEB) for the FseI enzyme is 5units per 1μg of dsDNA and the recommended maximum reaction volume is 50μl. The efficiency of the enzyme is higher in $\leq$ 50μl volumes. Therefore the following reaction solution was prepared:

- 1μg of dsDNA (purified PCR product)
- 1x CutSmart buffer (initial concentration 10x, catalog # B7204S, NEB)
- 20μg BSA (Bovin Serum Albumin), Molecular Biology Grade (initial concentration 20mg/ml, catalog # B9000S, NEB)
- 5 units of FesI restriction enzyme (initial concentration 2000units/ml, catalog # R0588S, NEB)
- Distilled water to adjust the reaction volume to 50μl (if required).

The reaction mix was then homogenized by a pipet and was incubated 4h at 37°. After incubation the restricted sample was purified using Monarch® PCR & DNA Cleanup Kit (5 μg) (catalog # T1030S) and was ready for ligation of two biotin modified DNA oligonucleotides: one (sur_compDNA2biot_MB) at the 3’ extremity of the leading strand and the other one (sur_DNAbiot_MB) at the 5’ extremity of the lagging strand.

A.2.3 Ligation of sur_DNAbiot_MB and sur_compDNA2biot_MB oligonucleotides

For successful ligation in reaction mix it is required to have DNA oligonucleotides 30 x in excess in molarity compared to restricted by FseI dsDNA product, e.g. for 1pmol dsDNA 30pmols of each oligonucleotide. Besides, as in the case of restriction, ligation enzymes act more efficiently in $\leq$50μl reaction volumes. To prepare 50μl reaction solution the following ingredients were mixed:

- 1pmol dsDNA (purified after the digestion by FseI)
- 30pmols sur_DNAbiot_MB (5'→3' Phosphate CCT-CTC-CTA-GCT-AGT-CTG-ATT-AGT-AGC-GCA-ZCA-GG-biot, Z = biotin-dT 684.70, Eurofins Genomics)
- 30pmols sur_compDNA2biot_MB (5'→3' GGC-CGG-AGA-GGA-TCG-ATC-AGA-CTA-ATC-ATC-GCG-ZAG-ZCC-biot, Z = biotin-dT 684.70, Eurofins Genomics)
- 1x T4 DNA ligase buffer (10x initial concentration, catalog # B0202S, NEB)
- 1812 units of T4 DNA ligase (with 400000units/ml initial concentration, catalog # M0202S, NEB)
- Distilled water to adjust the final volume to 50μl (if required)

The reaction solution was homogenized by a pipet and was incubated 4h at 37°. After incubation, the sample was purified using Monarch® PCR & DNA Cleanup Kit (5 μg) (catalog # T1030S) and was ready for the next restriction step: restriction by AflII restriction enzyme.

A.2.4 AflII restriction

Restriction of purified after ligation step dsDNA product generates four nucleotide long overhang (5'→3' TTAA) at the 5' end of the leading strand. For high efficiency of restriction, the recommended amount of AflII restriction enzyme (with initial concentration of 20000units/ml, catalog # R0520S, NEB) is 5-10units per 1μg of dsDNA, and the recommended volume is $\leq$50μl. In our case we prepared 50μl of reaction solution consisting of the following products:

- 1μg dsDNA (purified after ligation step)
- 1x (or 5μl) CutSmart buffer (initial concentration 10x, catalog # B7204S, NEB)
- 8 units of AflII restriction enzyme (initial concentration 20000units/ml, catalog # R0520S, NEB)
- 20μg BSA (Bovin Serum Albumin), Molecular Biology Grade (initial concentration 20mg/ml, catalog # B9000S, NEB)
- Distilled water to adjust the reaction volume to 50μl (if required)

Then the reaction solution was homogenized by a pipet and was incubated 4h at 37°. After the incubation, the reaction mix was purified using Monarch® PCR & DNA Cleanup Kit (5 μg) (catalog # T1030S, NEB) and was ready for Klenow Fragment (3'→5' exo-) enzyme (catalog # M0212S, NEB) treatment.

A.2.5 Klenow Fragment (exo-) treatment

After the restriction of dsDNA by AflII enxyme, the missing four nucleotides of the lagging strand (5'→3' TTAA) can be filled by another four nucleotides two of which (two adenines) are biotin modified. This filling can be done using Klenow Fragment (3'→5' exo-) enzyme (catalog # M0212S, NEB). The recommended reaction volumes are $\leq 50\mu$l. 50μl reaction solution was obtained by preparing a mixture of following products:

- 1μg dsDNA (purified after restriction by AflII enzyme)
- 3.76μl Biotin-14-dATP (initial concentration 0.4mM, catalog # 19524-016, Invitrogen©)
- 3μl mix of 1mM of each: dATP, dTTP, dGTP (catalog # N0446S, NEB)
- 5μl (1x) NEBuffer 2 (initial concentration 10x, catalog # B7002S, NEB)
- 6 units of Klenow Fragment (3'→5' exo-) (catalog # M0212S, NEB)
- Distilled water to adjust the reaction volume to 50μl (if required).

The reaction solution was then homogenized by a pipet and was incubated 30' at 37°. After incubation the enzyme was heat inactivated by incubating the sample for 20' at 75°. The sample then was purified by Monarch® PCR & DNA Cleanup Kit (5 μg) (catalog # T1030S) and was ready for optical trap experiments.

A.3 Preparation of RNA-DNA hybrid

The RNA-DNA hybrid with three biotin modified extremities was prepared in three steps. At first, a biotin modified dsDNA carrying the DNA strand of interest was prepared.Then, the RNA leading strand was prepared by in vitro transcription (IVT) and to finalize, the RNA strand and dsDNA were combined to do a strand exchange by hybridization. The dsDNA was prepared the same way as in "Preparation of dsDNA" (steps 1-5). The IVT of RNA strand and hybridization were done as follows:

A.3.1 In vitro transcription of RNA leading strand

2μg of purified PCR product was used for in vitro transcription (IVT) of the RNA leading strand using RiboMAX™Large Scale RNA Production Systems (catalog # P1300, Promega). The protocol is as follows. For 50μl reaction solution the following products were mixed:

- 2μg dsDNA (purified PCR product)
- 10 μl T7 RNA polymerase buffer (5x)

- 5 μl Enzyme mix (T7)
- 15 μl rNTP mix (rATP, rGTP, rCTP and rUTP, 25mM each)
- Distilled water to adjust the reaction volume to 50μl (if required)

The reaction mix was homogenized by a pipet and was incubated 3h at 37°.

To eliminate the ssDNA and dsDNA remained in the IVT product, 1.5μl RQ1 RNase-Free DNase (catalog # M6101, Promega) was added to the reaction solution. The latter was then incubated 15min at 37°C. After RQ1 digestion, the IVT product was purified by Monarch® Total RNA Miniprep Kit (catalog # T2010S, NEB, part 2 in the manual starting from step 3) and was ready to be hybridized with DNA lagging strand.

A.3.2 Hybridization

The recommended ssRNA : dsDNA ratio for hybridization is 1.5 : 1. This means for 1pmol dsDNA we will need 1.5pmols ssRNA. The recommended hybridization volume is $\leq$25μl. We chose the upper limit (25μl). Hybridization is performed in a special buffer (hybridization buffer), which consists of

- 50mM NaCl (catalog # S7653, Sigma-Aldrich)
- 10mM Hepes pH 7.6 (Hepes free acid, catalog # 391340-25GM, Sigma-Aldrich)
- 0.5mM EDTA (catalog # V4231, Promega)
- 12.5μl of 100% Formamid (50% of final volume, catalog # F9037, Sigma-Aldrich)

Afterwards the reaction solution was obtained by mixing

- 1pmol dsDNA* (purified after Klenow Fragment (3'$\rightarrow$ 5' exo-) treatment)
- 1.5pmols ssRNA (purified IVT product)
- Hybridization buffer to obtain 25μl final volume

The required concentration of dsDNA is usually obtained in big volumes. To avoid adjusting the concentration of the hybridization buffer (in order to obtain 25μl final volume), it is better to concentrate or even dry the dsDNA beforehand in the reaction tube a using vacuum centrifuge, and then to add ssRNA and the hybridization buffer into the tube.

The final reaction mix was then gently homogenized by a pipet and went through following thermal cycle:
98°C $\rightarrow$ 1'
65°C $\rightarrow$ 15'
60°C $\rightarrow$ 15'
55°C $\rightarrow$ 5'

50°C → 5'
40°C → 5'
30°C → 5'
20°C → 5'

After hybridization, the remaining in the reaction mix dsDNA and ssDNA were digested using EcoRI-HF® restriction enzyme in 50μl reaction volume. The new reaction solution consists of:

- 25μl reaction mix (after hybridization)
- 5μl CutSmart® Buffer (initial concentration 10x, catalog # B7204S, NEB)
- 1μl EcoRI-HF® restriction enzyme (initial concentration 20000units/ml, catalog # R3101S, NEB)
- 19μl Distilled water to adjust the reaction volume to 50μl

The restriction was performed incubating the reaction mix 15' at 37°C. EcoRI-HF® was inactivated by a second incubation 20' at 65°C. The sample was then purified using Microspin™G-50 Columns (catalog # GE27-5330-01, Sigma-Aldrich) and was obtained a hybrid molecule (RNA-DNA) with biotin modifications at both extremities of DNA lagging strand. This sample was then ready for the final step: the ligation of biotin modified RNA oligonucleotide to RNA 3' extremity.

A.3.3 Ligation of sur_RNAbiot_MB Ph

Ligation of sur_RNAbiot_MB Ph oligonucleotide (5'→3' Phosphate_GCG-CAZ-CAG-G, Z = biotin-dT 684.70) is performed in 100μl reaction volume. The reaction mix components are the followings:

- 1pmol RNA-DNA hybrid (after hybridization)
- 0.22pmols sur_RNAbiot_MB oligonucleotide
- 10μl T4 Rnl2 Reaction Buffer (initial concentration 10x, supplied with T4 RNA Ligase 2 (dsRNA Ligase))
- 70units of T4 RNA Ligase 2 (dsRNA Ligase, initial concentration 10000units/ml, catalog # M0239S, NEB)
- Distilled water to adjust the reaction volume to 100μl (if required)

The reaction solution was then gently homogenized by a pipet and was incubated for 4h at 37°. After the incubation, the non incorporated biotin modified oligonucleotides were removed by Microspin™G-50 Columns (catalog # GE27-5330-01, Sigma-Aldrich) and the sample was ready for optical trap experiment.

A.4 Preparation of dsRNA

The dsRNA with biotin modifications at the 5' and 3' extremities of its lagging strand and at the 3' extremity of its leading strand was prepared in two steps. At first, the leading strand was produced and then the lagging strand. The RNA leading strand was prepared by IVT, the same way as in "Preparation of RNA-DNA hybrid" (step 1). The lagging RNA strand was prepared as follows.

A.4.1 PCR

The sequence of interest containing the genes rrlB (coding for 23S rRNA), rrfB (coding for 5S rRNA) and one half of murB, was amplified by PCR from pT7-rrnB plasmid. The PCR primers were designed to introduce a restriction sites for AflII and FseI restriction enzymes at one and the other extremity of PCR product (same as for RNA-DNA) and a T7 RNA polymerase promoter sequence at the opposite extremity of PCR product compared to RNA-DNA case. The T7 RNA polymerase promotor sequence in this extremity allows to in-vitro transcribe the lagging RNA strand. For 250μl PCR the following reaction mix was prepared:

- 12.5μl of 10μM ÊF PCR TB forward primer (5'→3' TAA-TAC-GAC-TCA-CTA-TAG-GGA-GA-GGC-CGG C-CCA-GAC-GAG-TTA-AGT-CAC-CAT-AC, Eurogentec)
- 12.5μl of 10μM RME PCR TB reverse primer (5'→3' C (2'OMeRNA)U (2'OMeRNA) A- AGC-GTA-CAC GG TGG ATG, Eurogentec)
- 5μl mix of 10mM each dATP, dGTP, dCTP, dTTP (catalog # N0446S, NEB)
- 2μl of pT7-RB plasmid (IBPC) with concentration of 16.3ng/μl
- 2.5μl Q5® High-Fidelity DNA Polymerase with 2000units/ml concentration (catalog # M0491S, New England Biolabs)
- 50μl of Q5® Reaction Buffer (initial concentration 5x) to have 1x final concentration (catalog # B9027S, New England biolabs)
- 50μl of 5M Betaine solution (catalog # B0300-1VL, Sigma Aldrich)
- 4μl of ET-SSB single-stranded DNA binding protein with concentration of 500μg/ml (catalog # M2401S, New England Biolabs)
- 111.5μl of distilled water.

The reaction solution was homogenized gently with a pipet and distributed into five 200μl PCR tubes to have 50μl solution in each. The tubes were incubated in the thermo-cycler and went through the following thermal cycle:

98°C: 30"

98°C: 10”
66°C: 30” x 30
72°C: 1’30”
72°C: 5’

After incubation the PCR product was purified using Monarch® PCR & DNA Cleanup Kit (5 μg) (catalog # T1030S).

Part of the purified PCR product (dsDNA of 4050bp) was used for IVT of the lagging RNA strand.

A.4.2 In vitro transcription of RNA lagging strand

For in vitro transcription (IVT) of the RNA lagging strand the RiboMAX™Large Scale RNA Production Systems (catalog # P1300, Promega) was used with a modified rNTP concentrations. The protocol is as follows. For 50μl reaction solution the following products were mixed:

- 2μg dsDNA (purified PCR product)
- 10 μl T7 RNA polymerase buffer (5x)
- 5 μl Enzyme mix (T7)
- 15 μl rNTP mix ([rATP] = [rCTP] = [rUTP] = 7.5mM, [rGTP] = 0.6mM, [rGMP] = 6mM)
- Distilled water to adjust the reaction volume to 50μl (if required)

The reaction mix was homogenized by a pipet and was incubated 3h at 37°C.

To eliminate the ssDNA and dsDNA remaining in the IVT product, 1.5μl RQ1 RNase-Free DNase (catalog # M6101, Promega) was added to the reaction solution. The latter was then incubated 15min at 37°C. After RQ1 digestion, the IVT product was purified by NucleoSpin® RNA Clean-up kit (catalog # 740948.10, Macherey Nagel) and was ready for hybridization with two DNA oligonucleotides, the latter serving as bridges for ligation of biotin modified RNA oligonucleotides.

A.4.3 Hybridization of DNA and ligation of RNA oligonucleotides

The biotin modification of the 5’ and 3’ extremities of the RNA lagging strand was done by ligation of two biotin modified RNA oligonucleotides. There is one obstacle however. T4 RNA ligase 2 performs efficient ligation of RNA oligonucleotides only to the sticky ends of a dsRNA or a DNA-RNA hybrid. Creating hybrid regions (with sticky ends) by hybridization of two DNA oligonucleotides at both extremities of RNA lagging strand eliminated this problem. The protocol for hybridization of DNA oligonucleotides is as follows. For 18μl of reaction solution were mixed:

- 3μg RNA lagging strand (purified IVT product)

- 1.1μM (in final volume) RNA 5 TB oligonucleotide (5'→3' Biotin-CCZ-GAZ-GCG-CUA-CUA-AUC-AGA-CUA-GCU-A, Z = biotin-dT, Eurogentec)

- 1.1μM (in final volume) RNA 3 TB oligonucleotide (5'→3' Phosphate - UCG-CUU-AAC-CCU-Z A A - Biotin, Z = biotin-dT, Eurogentec)

- 0.55μM (in final volume) DNA SPL5 TB oligonucleotide (5'→3' CGC-CCT-CTC-CTA-GCT-AGT-CT, Eurogentec)

- 0.55μM (in final volume) DNA SPL3 TB oligonucleotide (5'→3' G-GTT-AAG-CGA-CTA- AGC-GTA-C, Eurogentec)

- 75mM KCl (in final volume) (cas # 7447-40-7, Acros Organics, Fisherscientific)

- 10mM Hepes pH = 7.5 (in final volume)

The reaction was homogenized by a pipette and was incubated using the following slow cooling hybridization protocol:

95°C: 1'
70°C: 3'
65°C: 3'
60°C: 3'
55°C: 3'
50°C: 3'
45°C: 3'
40°C: 3'
35°C: 3'
30°C: 3'
25°C: 3'

After hybridization 12μl of the product was used to prepare a reaction solution for RNA oligonucleotides ligation. The protocol of ligation mixture is as follows:

- 1.5μl T4 RNA Ligase 2 (dsRNA ligase, initial concentration 10000units/ml, catalog # M0239S, NEB)

- 1.5μl T4 Rnl2 Reaction Buffer (initial concentration 10x, supplied with T4 RNA ligase 2)

The reaction solution was homogenized by a pipet and was incubated for 1h at 37°. The reaction was stopped by adding EDTA (13mM final concentration, catalog # V4231, Promega) and was purified using Microspin^{TM}G-50 Columns (catalog # GE27-5330-01, Sigma-Aldrich). This way we obtained an RNA lagging strand with biotin modifications at its two extremities, which is ready to be hybridized with RNA leading strand.

A.4.4 Hybridization of two RNA strands

For hybridization it was prepared 30μl of reaction mix containing:

1μg RNA lagging strand (purified after splint ligation) 2μg RNA leading strand (purified IVT product) 75mM KCl (cas # 7447-40-7, Acros Organics, Fisherscientific) 10mM Hepes pH = 7.5

The reaction solution was homogenized by a pipet and was incubated using the following slow cooling hybridization protocol:

90°C: 1'
85°C: 2'
80°C: 2'
75°C: 2'
70°C: 3'
65°C: 3'
60°C: 3'
55°C: 3'
50°C: 3'
45°C: 3'
40°C: 3'
35°C: 3'
30°C: 3'
25°C: 3'

Once hybridization was done, a dsRNA with biotin modified lagging strand was obtained.

A.4.5 Ligation of sur_RNAbiot_MB Ph

The final dsRNA construct, with biotin modifications at its 3 extremities, was obtained by ligating biotin modified sur_RNAbiot_MB Ph RNA oligonucleotide to 3' extremity of the leading strand. For ligation efficiency the ligation reaction reaction solution should contain RNA oligonucleotide with concentration (in molarity)10x prior to dsRNA concentration. The ligation protocol is as follows. For 15μl of reaction solution the following ingredients were mixed:

- 0.16pmol dsRNA (after hybridization)
- 1.6pmol sur_RNAbiot_MB Ph oligonucleotide (5'→3' Phosphate GCG-CAZ-CAG-G, Z = biotin-dT 684.70)
- 1.5μl T4 RNA Ligase 2 (dsRNA ligase, initial concentration 10000units/ml, catalog # M0239S, NEB)
- 1.5μl T4 Rnl2 Reaction Buffer (initial concentration 10x, supplied with T4 RNA ligase 2)

The reaction solution was homogenized by a pipet and was incubated for 1h at 37°C. The reaction was stopped by EDTA (catalog # V4231, Promega) addition (with 13mM final concentration). The sample was then purified using Microspin™G-50 Columns (catalog # GE27-5330-01, Sigma-Aldrich) and was ready for optical trap experiments.

A.5 Preparation of DNA-RNA hybrid

The preparation of the DNA-RNA hybrid with biotin modifications at its 3 extremities was done in three steps. A biotin modified dsDNA carrying the DNA strand of interest was prepared as in "Preparation of dsDNA" (steps:1-5). Then, the RNA lagging strand was prepared by IVT and splint ligation, as in "Preparation of dsRNA" (steps 1-3). At the end, the dsDNA and the RNA strand were combined to do a strand exchange using the same hybridization protocol as in "Preparation of RNA-DNA hybrid" (step 2). The final DNA-RNA product was purified using Microspin™ G-50 Columns (catalog # GE27-5330-01, Sigma-Aldrich) and then was ready for optical trap experiments.

A.6 Preparation of 23S rRNA

A.6.1 Polymerase chain reaction (PCR)

The sequence of interest (2904bp) containing the gene rrlB (coding for 23S rRNA), was amplified by polymerase chain reaction (PCR) from a pT7-rrnB plasmid. The PCR primers were designed such that one of them (F-MB forward primer) introduces a sequence of T7 RNA polymerase and a restriction site for AflII restriction enzyme in one extremity of PCR product. The PCR yield and stability were improved by addition of Betaine (1M final concentration) and single-stranded DNA binding protein ET-SSB (200ng final amount). For 500μl of PCR reaction was prepared a solution containing the following components:

- 25μl of 10μM F_MB forward primer (5'→3' TAA-TAC-GAC-TCA-CTA-TAG-GGA-GA-C-AAT-TG-C-TTA-AG-G-GTT-AAG-CGA-CTA- AGC-GTA-C, Eurogentec)
- 2.5μl of 100μM 23S R_MB reverse primer (5'→3' AAG-GTT-AAG-CCT-CAC-GGT-T, Eurogentec)
- 10μl mix of 10mM each dATP, dGTP, dCTP, dTTP (catalog # N0446S, NEB)
- 4μl of pT7-RB plasmid (IBPC) with concentration of 16.3ng/μl
- 5μl Q5® High-Fidelity DNA Polymerase with 2000units/ml concentration (catalog # M0491S, New England Biolabs)
- 100μl of Q5® Reaction Buffer (initial concentration 5x) to have 1x final concentration (catalog # B9027S, New England biolabs)

- 100μl of 5M Betaine solution (catalog # B0300-1VL, Sigma Aldrich)
- 8μl of ET-SSB single-stranded DNA binding protein with concentration of 500μg/ml (catalog # M2401S, New England Biolabs)
- 245.5μl of distilled water.

The reaction solution was gently homogenized with a pipet and then distributed into ten 200μl PCR tubes to have 50μl solution in each. The tubes with the reaction mix were then incubated in the thermo-cycler and went through the following thermal cycle:

98°C: 30”
98°C: 10”
66°C: 30” x 30
72°C: 1’30”
72°C: 5’

After incubation the PCR product was purified using Monarch® PCR & DNA Cleanup Kit (5 μg) (catalog # T1030S) and was ready for in vitro transcription of 23S rRNA.

A.6.2 In vitro transcription of 23S rRNA

The 23S rRNA was in vitro transcribed using RiboMAX™Large Scale RNA Production Systems (catalog # P1300, Promega). The protocol is as follows. For 50μl reaction solution the following reaction mix was used:

- 2μg dsDNA (purified PCR product)
- 10 μl T7 RNA polymerase buffer (5x)
- 5 μl Enzyme mix (T7)
- 15 μl rNTP mix (rATP, rGTP, rCTP and rUTP, 25mM each)
- Distilled water to adjust the reaction volume to 50μl (if required)

The reaction mix was gently homogenized by a pipet and was incubated 3h at 37°C.

The IVT product was purified and the ssDNA and dsDNA were eliminated by Monarch® Total RNA Miniprep Kit (catalog # T2010S, NEB, manual -> part 2 starting from step 3). The 23S rRNA was then ready for optical trap experiments with early binding ribosomal proteins. To avoid introducing in the experiment the particles released from the purification membrane, the 23S rRNA solution was first centrifuged 5’ at 16000G and a certain amount (correlated with the final concentration of ribosomal proteins) from the upper level of the supernatant was added to the final experimental mix.

Bibliography

References are given separately for the introductory parts, and the articles.
Where available, links point to the publisher's website as provided by the
doi system. Further links point to the position in the thesis where they are referenced.

References for the Introduction and Chapters 1-2

[1] Daniel S. Johnson, Lu Bai, Benjamin Y. Smith, Smita S. Patel and Michelle D. Wang, *Single-molecule studies reveal dynamics of DNA unwinding by the ring-shaped T7 helicase*, Cell **129** (2007) 1299–1309. (document), III.1

[2] J. F. Allemand, D. Bensimon, R. Lavery and V. Croquette, *Stretched and overwound dna forms a pauling-like structure with exposed bases*, PNAS **95** (1998) 14152–14157. (document), III.1

[3] J. F. Léger, G. Romano, A. Sarkar, J. Robert, L. Bourdieu, D. Chatenay and J. F. Marko, *Structural transitions of a twisted and stretched dna molecule*, Phys. Rev. Lett. **83** (1999) 1066–1069. (document), III.1

[4] Douglas E. Smith, Sander J. Tans, Steven B. Smith, Shelley Grimes, Dwight L. Anderson and Carlos Bustamante, *The bacteriophage $\phi 29$ portal motor can package dna against a large internal force*, Nature **413** (2001) 748–752. (document), III.1

[5] John Peter Rickgauer, Derek N. Fuller, Shelley Grimes, Paul J. Jardine, Dwight L. Anderson and Douglas E. Smith, *Portal motor velocity and internal force resisting viral dna packaging in bacteriophage $\phi 29$*, Biophysical Journal **94** (2008) 159–167. (document), III.1

[6] Susanne Spillmann, Ferdinand Dohme and Knud H. Nierhaus, *Assembly in vitro of the 50 S subunit from escherichia coli ribosomes: Proteins essential for the first heat-dependent conformational change*, Journal of Molecular Biology **115** (1977) 513 – 523. (document), II

[7] Susana M. Cerritelli and Robert J. Crouch, *Ribonuclease H: the enzymes in eukaryotes*, The FEBS Journal **276** (2009) 1494–1505. I.1.1

[8] Corina Ohle, Rafael Tesorero, Géza Schermann, Nikolay Dobrev, Irmgard Sinning and Tamás Fischer, *Transient rna-dna hybrids are required for efficient double-strand break repair*, Cell **167** (2016) 1001–1013.e7. I.1.1

[9] Leonardo A. Ambrosio and Hugo E. Hernández-Figueroa, *Fundamentals of negative refractive index optical trapping: forces and radiation pressures exerted by focused gaussian beams using the generalized lorenz-mie theory*, Biomed. Opt. Express **1** (2010) 1284–1301. I.2.1

[10] A. Ashkin, *Acceleration and trapping of particles by radiation pressure*, Phys. Rev. Lett. **24** (1970) 156–159. I.2.1

[11] A Ashkin, *Forces of a single-beam gradient laser trap on a dielectric sphere in the ray optics regime*, Biophysical Journal **61** (1992) 569–582. I.2.1

[12] Pierre Mangeol, *Interaction entre la protéine ribosomique L20 et l'ARN 23S : sondage direct par pièges optiques*, PhD thesis, Paris 6, 2009. I.2.2

[13] K.H. Nierhaus, *The assembly of prokaryotic ribosomes*, Biochimie **73** (1991) 739 – 755. II

[14] Knud H. Nierhaus and Ferdinand Dohme, *Total reconstitution of functionally active 50s ribosomal subunits from escherichia coli*, Proceedings of the National Academy of Sciences of the United States of America **71** (1974) 4713–4717. II

[15] Ferdinand Dohme and Knud H. Nierhaus, *Total reconstitution and assembly of 50 s subunits from escherichia coli ribosomes in vitro*, Journal of Molecular Biology **107** (1976) 585 – 599. II

[16] Knud H. Nierhaus and Ferdinand Dohme, *Total reconstitution of 50 S subunits from escherichia coli ribosomes*, in *Nucleic Acids and Protein Synthesis Part G*, Volume *59* of *Methods in Enzymology*, pages 443 – 449, Academic Press, 1979. II

[17] R Röhl and Knud H Nierhaus, *Assembly map of the large subunit (50s) of escherichia coli ribosomes*, PNAS **79** (1982) 729–733. II, II

[18] M. Herold and K. H. Nierhaus, *Incorporation of six additional proteins to complete the assembly map of the 50 s subunit from escherichia coli ribosomes*, Journal of Biological Chemistry **262** (1987) 8826–33. II

[19] Nenad Ban, Poul Nissen, Jeffrey Hansen, Peter B. Moore and Thomas A. Steitz, *The complete atomic structure of the large ribosomal subunit at 2.4 å resolution*, Science **289** (2000) 905–920. II

[20] Joerg Harms, Frank Schluenzen, Raz Zarivach, Anat Bashan, Sharon Gat, Ilana Agmon, Heike Bartels, François Franceschi and Ada Yonath, *High resolution structure of the large ribosomal subunit from a mesophilic eubacterium*, Cell **107** (2001) 679 – 688. II

[21] Maria Selmer, Christine M. Dunham, Frank V. Murphy, Albert Weixlbaumer, Sabine Petry, Ann C. Kelley, John R. Weir and V. Ramakrishnan, *Structure of the 70s ribosome complexed with mrna and trna*, Science **313** (2006) 1935–1942. II

[22] Sebastian Klinge, Felix Voigts-Hoffmann, Marc Leibundgut and Nenad Ban, *Atomic structures of the eukaryotic ribosome*, Trends in Biochemical Sciences **37** (2012) 189–198. II

[23] Gulnara Yusupova and Marat Yusupov, *High-resolution structure of the eukaryotic 80s ribosome*, Annual Review of Biochemistry **83** (2014) 467–486. II

[24] Joseph H. Davis and James R. Williamson, *Structure and dynamics of bacterial ribosome biogenesis*, Philosophical Transactions of the Royal Society of London B: Biological Sciences **372** (2017). II

[25] S L Gotta, O L Miller and S L French, *rRNA transcription rate in escherichia coli.*, Journal of Bacteriology **173** (1991) 6647–6649. II, II

[26] Olivier Cordin, Josette Banroques, N. Kyle Tanner and Patrick Linder, *The dead-box protein family of rna helicases*, Gene **367** (2006) 17 – 37. II

[27] Isabelle Iost, Thierry Bizebard and Marc Dreyfus, *Functions of dead-box proteins in bacteria: Current knowledge and pending questions*, Biochimica et Biophysica Acta (BBA) - Gene Regulatory Mechanisms **1829** (2013) 866 – 877. II

[28] Zahra Shajani, Michael T. Sykes and James R. Williamson, *Assembly of bacterial ribosomes*, Annual Review of Biochemistry **80** (2011) 501–526. II

[29] Robert A. Britton, *Role of gtpases in bacterial ribosome assembly*, Annual Review of Microbiology **63** (2009) 155–176. II

[30] J. R. Williamson, *After the ribosome structures: How are the subunits assembled?*, RNA **9** (2003) 165–167. II

[31] Mathilde Bercy, *Structures secondaires dans l'ARN: une étude par mesure de forces sur molécules uniques*, PhD thesis, PSL Research University, 2015. II, A.1

[32] Laurent Geffroy, *Interactions between 23S RNA and proteins uL24 and uL4 during the assembly of the large ribosomal subunit: force measurements by optical tweezers*, PhD thesis, PSL Research University, 2017. A.1

Additional References in Paper 1

[33] Essevaz-Roulet B, Bockelmann U, Heslot F (1997) Mechanical separation of the complementary strands of DNA. Proc. Natl. Acad. Sci. USA 94:11935-11940.

[34] Liphardt J, Onoa B, Smith SB, Tinocco I, Bustamante C (2001) Reversible unfolding of single RNA molecules by mechanical force. Science 292:733-737.

[35] Bockelmann U, Thomen P. Essevaz-Roulet B, Viasnoff V, Helot F (2002) Unzipping DNA with optical tweezers:high sequence sensitivity and force flips. Biophys J 82:1537-1553.

[36] Gross P, Laurens N, Oddershede LB, Bockelmann U, Peterman EJG, Wuite GJL (2011) Quantifying how DNA stretches, melts and changes twist under tension. Nature Physics 7:731-736.

[37] Cluzel P, Lebrun A, Heller C, Lavery R, Viovy JL, Chatenay D, Caron F (1996) DNA:an extensible molecule. Science 271:792-794.

[38] Smith S B, Cui Y, Bustamante C (1996) Overstretching B-DNA:the elastic response of individual double-stranded and single-stranded DNA molecules. Science 271:795-799.

[39] Bustamante C, Smith S B, Liphardt J, Smith D (2000) Single-molecule studies of DNA mechanics. Curr. Opin. Struct. Biol. 10:279-285.

[40] King GA, Gross P, Bockelmann U, Modesti M, Wuite GJL, Peterman EJG (2013) Revealing the competition between peeled ssDNA, melting bubbles and S-DNA during DNA overstretching using fluorescence microscopy. Proc. Natl. Acad. Sci. USA 110:3859-3864.

[41] Zhang X, Chen H, Le S, Rouzina I, Doyle P S, Yan J (2013) Revealing the competition between peeled ssDNA, melting bubbles, and S-DNA during DNA overstretching by single-molecule calorimetry. Proc. Natl. Acad. Sci. USA 110:3865-3870.

[42] Paik DH, Perkins TT (2011) Overstreching DNA at 65 pN does not require peeling from free ends or nicks. J. Am. Chem. Soc. 133:3219-3221.

[43] Geffroy L, Mangeol P, Bizebard T, Bockelmann U (2017) RNA unzipping and force measurements with a dual optical trap. Methods Mol. Biol. 1665:25-41.

[44] Gittes F, Schmidt C F (1998) Interference model for back-focal-plane displacement detection in optical tweezers. Opt. Lett. 23:7-9.

[45] Neuman K, Block S M (2004) Optical trapping. Rev. Sci. Instrum. 75:2787-2809.

[46] Mangeol P, Bockelmann U (2008) Interference and crosstalk in double optical tweezers using a single laser source. Rev. Sci. Instrum 79:083103.

[47] Dean M (1987) Determining the hybridization temperature for Si nuclease mapping. Nucleic Acids Res. 15:6754.

[48] Vilfan I D, Kamping W, van den Hout M, Candelli A, Hage S, Dekker N H (2007) An RNA toolbox for single-molecule force spectroscopy studies. Nucleic Acids Res. 35:6625-6639.

[49] Odijk T (1995) Stiff chains and filaments under tension. Macromolecules 28:7016-7018.

[50] Xia T, SantaLucia Jr J, Burkard M E, Kierzek R, Schroeder S J, Jiao X, Cox C, Turner D H (1998) Thermodynamic parameters for an expanded nearest-neighbor model for formation of RNA duplexes with Watson-Crick base pairs. Biochemistry 37:14719-735.

[51] SantaLucia Jr J (1998) A unified view of polymer, dumbbell, and oligonucleotide DNA nearest-neighbor thermodynamics. Proc. Natl. Acad. Sci. USA 95:1460-65.

[52] Sugimoto N, Nakano S, Katoh M, Matsumura A, Nakamuta H, Ohmichi T, Yoneyama M, Sasaki M (1995) Thermodynamic parameters to predict stability of RNA/DNA hybrid duplexes. Biochemistry 34:11211-216. bibitemub1998 Bockelmann U, Essevaz-Roulet B, Heslot F (1998) DNA strand separation studied by single molecule force measurements. Phys. Rev. E 58:2386-2394.

[53] Marin-Gonzalez A, Vilhena J G, Perez R, Moreno-Herrero F (2017) Understanding the mechanical response of double-stranded DNA and RNA under constant stretching forces using all-atom molecular dynamics. Proc. Natl. Acad. Sci. USA 114:7049-7054.

[54] Bercy M, Bockelmann U (2015) Hairpins under tension:RNA versus DNA. Nucleic Acids Res. 43:9928-9936.

[55] Herrero-Galán E H, Fuentes-Perez M E, Carrasco C, Valpuesta J M, Carrascosa J L, Moreno-Herrero F, Arias-Gonzalez J R (2012) Mechanical identities of RNA and DNA double helices unveiled at the single-molecule level. J. Am. Chem. Soc. 135:122-131.

[56] Roca-Cusachs P, Conte V, Trepat X (2017) Quantifying forces in cell biology. Nat. Cell Biol. 19:742-751.

[57] Nicklas R B (1983) Measurements of the force produced by the mitotic spindle in anaphase. J. Cell Biol. 97:542-548.

[58] Smith D E, Tans S J, Smith S B, Grimes S, Anderson D L, Bustamante C (2001) The bacteriophage ϕ29 portal motor can package DNA against a large internal force. Nature 413:748-752.

[59] Rickgauer J P, Fuller D N, Grimes S., Jardine P J, Anderson D L, Smith D E (2008) Portal motor velocity and internal force resisting viral DNA packaging in bacteriophage ϕ29. Biophys. J. 94:159-167.

[60] Harlepp S, Marchal T, Robert J, Léger J-F, Xayaphoummine A, Isambert H, Chatenay D (2003) Probing complex RNA structures by mechanical force. Eur. Phys. J. E 12:605-615.

[61] Mangeol P, Bizebard T, Chiaruttini C, Dreyfus M, Springer M, Bockelmann U (2011) Probing ribosomal protein-RNA interactions with an external force. Proc. Natl. Acad. Sci. 108:18272-18276.

[62] Kaczanowska M, Rydén-Aulin M (2007) Ribosome biogenesis and the translation process in *Escherichia coli*. Microbiol. Mol. Biol. Rev. 71:477-494.

[63] Kozak M (2005) Regulation of translation via mRNA structure in prokaryotes and eukaryotes. Gene 361:13-37.

[64] Jacobs E, Mills J D, Janitz M (2012) The role of RNA structure in posttranscriptional regulation of gene expression. J. Genet. Genomics 39:535-543.

[65] Lorsch J R (2002) RNA chaperones exist and DEAD box proteins get a life. Cell 109:797-800.

[66] Liu T, Kaplan A, Alexander L, Yan S, Wen J-D, Lancaster L, Wickersham C E, Fredrick K, Noller H, Tinoco Jr I, Bustamante C J (2014) Direct measurement of the mechanical work during translocation by the ribosome. eLife 3:e03406.

[67] Schuwirth B S, Borovinskaya M A, Hau C W, Zhang W, Vila-Sanjurjo A, Holton J M, Cate J H D (2005) Structures of the bacterial ribosome at 3.5 Å resolution. Science 310:827-834.

Additional References in Paper 2

[68] Single molecule techniques: a laboratory manual, Eds. P. Selvin and T. Ha, Cold Spring Harbor Laboratory Press, NY 2008

[69] Single molecule analysis, Methods in Molecular Biology 783, Eds. E. Peterman and G. Wuite, Humana Press NY 2011

[70] S. B. Smith, L. Finzi, C. Bustamante: Direct mechanical measurements of the elasticity of single DNA molecules by using magnetic beads. Science 258, 1122-1126 (1992)

[71] K. Svoboda, C. F. Schmidt, B. J. Schnapp, S. M. Block: Direct observation of kinesin stepping by optical trapping interferometry. Nature 365, 721-727 (1993)

[72] T. R. Strick, V. Croquette, D. Bensimon: Single-molecule analysis of DNA uncoiling by a type II topoisomerase. Nature, 404, 901-904 (2000)

[73] H. Yin, M. D. Wang, K. Svoboda, R. Landick, S. M. Block, J. Gelles: Transcription against an applied force. Science 270, 1653-1657 (1995)

[74] Wen J-D, Lancaster L, Hodges C, Zeri A-C, Yoshimura S H, Noller H F, Bustamante C, Tinocco Jr I (2008) Following translation by single ribosomes one codon at a time. Nature 452: 598-603.

[75] Liu T, Kaplan A, Alexander L, Yan S, Wen J-D, Lancaster L, Wickersham C E, Fredrick K, Noller H, Tinoco Jr I, Bustamante C J (2014) Direct measurement of the mechanical work during translocation by the ribosome. eLife 3: e03406.

[76] X. Qu, J.-D. Wen, L. Lancaster, H. F. Noller, C. Bustamante, I. Tinoco: The ribosome uses two active mechanisms to unwind messenger RNA during translation. Nature 475, 118-21 (2011)

[77] X. Qu, L. Lancaster, H. F. Noller, C. Bustamante, I. Tinoco: Ribosomal protein S1 unwinds double-stranded RNA in multiple steps. Proc. Natl. Acad. Sci. USA 109, 14458-63 (2012)

[78] X. Zhuang, L. E. Bartley, H. P. Babcock, R. Russel, T. Ha, D. Herschlag, S. Chu: A single-molecule study of RNA catalysis and folding. Science 288, 2048-2051 (2000)

[79] H. D. Kim, G. U. Nienhaus, T. Ha, J. W. Orr, J. R. Williamson, S. Chu: Mg2+-dependent conformational change of RNA studied by fluorescence correlation and FRET on immobilized single molecules. Proc. Natl. Acad. Sci. USA 99, 4284-4289 (2002)

[80] S. Spillmann, F. Dohme, K. H. Nierhaus: Assembly in vitro of the 50S subunit from Escherichia coli ribosomes: Proteins essential for the first heat dependent conformational change. J. Mol. Biol. 115, 513-523 (1977)

[81] S. S. Chen and J. R. Williamson: Characterization of the ribosome biogenesis landscape in E. coli using quantitative mass spectrometry. J. Mol. Biol. 425, 767-779 (2013)

[82] B. T. U. Lewicki, T. Margus, J. Remme, K. H. Nierhaus: Coupling of rRNA transcription and ribosomal assembly *in vivo*. J. Mol. Biol. 231, 581-593 (1993)

[83] R. Nicolay, T. Hilal, B. Qin, T. Mielke, J. Bürger, J. Loerke, K. Textoris-Taube, K. H. Nierhaus, C. M. T. Spahn: Structural visualization of the formation and activation of the 50S ribosomal subunit during *in vitro* reconstitution. Mol. Cell. 70, 881-893 (2018)

[84] Y. Shimizu, A. Inone, Y. Tomari, T. Suzuki, T. Yokogawa, K. Nishikawa, T. Ueda: Cell-free translation reconstituted with purified components. Nat. Biotechnol. 19, 751-755 (2001)

[85] Y. Shimizu, T. Kanamori, T. Ueda: Protein synthesis by pure translation systems. Methods 36, 299-304 (2005)

[86] Haentjens-Sitri J, Allemand F, Springer M, Chiaruttini C (2008) A competition mechanism regulates the translation of the *Escherichia coli* operon encoding ribosomal proteins L35 and L20. J Mol Biol 375: 612-625.

[87] Raibaud S, et al. (2002) NMR structure of bacterial ribosomal protein L20: implications for ribosome assembly and translational control. J Mol Biol 323:143-151.

[88] Raibaud S, et al. (2003) How bacterial ribosomal protein L20 assembles with 23 S ribosomal RNA and its own messenger RNA. J Biol Chem 278:36522-36530.

[89] Timsit Y, Allemand F, Chiaruttini C, & Springer M (2006) Coexistence of two protein folding states in the crystal structure of ribosomal protein L20. EMBO Rep 7:1013-1018.

[90] Selmer M, et al. (2006) Structure of the 70S ribosome complexed with mRNA and tRNA. Science 313:1935-1942.

[91] Guillier M, et al. (2005) The N-terminal extension of Escherichia coli ribosomal protein L20 is important for ribosome assembly, but dispensable for translational feedback control. RNA 11:728-738.

[92] S. L. Gotta, O. L. Miller JR., S. L. French: rRNA transcription rate in *Escherichia coli*. J. Bacteriol. 173, 6647-6649 (1991)

[93] L. Geffroy, T. Bizebard, R. Aoyama, T. Ueda, U. Bockelmann: Force measurements show that uL4 and uL24 cooperatively stabilize a fragment of 23S rRNA essential for ribosome assembly. Manuscript submitted for publication.

[94] K. H. Nierhaus and F. Dohme: Total reconstitution of functionally active 50S ribosomal subunits from *E. coli*. Proc. Natl. Acad. Sci. USA 71, 4713-4717 (1974)

[95] K. H. Nierhaus: The assembly of prokaryotic ribosomes. Biochimie 73, 739-755 (1991)

[96] R. Röhl, H. E. Roth, K.H. Nierhaus: Inter-protein dependences during assembly of the 50S subunit from *Escherichia coli* ribosomes. Z. Physiol. Chem. 363, 143-157 (1982)

[97] T. Ueda et al: Unpublished result presented at the Tokyo meeting of our Human Frontier project. (2018)

[98] K. H. Nierhaus: Bacterial ribosomes: assembly. In eLS. John Wiley & Sons Ltd, Chichester. http//www.els.net [doi: 10.1038/npg.els.0003947]

[99] Viasnoff V, Meller A, Isambert H (2006) DNA nanomechanical switches under folding kinetics control. Nanoletters 6: 101-104.

Résumé

L'ADN et l'ARN double brin (ADNdb, ARNdb) subissent des transitions de surétirement avec des forces d'environ 60 pN. Nous effectuons des mesures de force à l'aide d'un piège optique à double faisceau contenant deux billes reliées par une seule molécule. Un brin du duplex est attaché aux deux extrémités aux deux billes, tandis que l'autre brin n'est attaché qu'à une seule extrémité. Quatre cas différents sont comparés: ADNdb, ARNdb, hybride ARN-ADN avec ADN sous tension et hybride ADN-ARN avec ARN sous tension.

Un surétirement se produit pour les quatre duplex. La différence la plus remarquable est que les ARNdb présentent un plateau lisse, alors que les autres duplex présentent des motifs en dents de scie. Nous constatons que les ARNdb s'étirent par un mécanisme différent et expliquons pourquoi cette propriété pourrait aider les structures d'ARN à s'assembler et à jouer leurs rôles biologiques.

Un surétirement de l'hybride ARN-ADN libère progressivement un brin d'ARN. Les structures formées au sein de cet ARN naissant sont visibles dans le signal de force lors du re-recuit. Pour la première fois à notre connaissance, nous imitons donc et étudions le repliement de l'ARN co-transcriptionnel dans un test in vitro. En se concentrant sur le stade précoce de l'assemblage des grandes sous-unités ribosomales de E. coli (domaines I-II de l'ARNr 23S et des protéines r L4, L13, L20, L22, L24), on observe plus souvent un recuit partiel avec les protéines r. Nos résultats indiquent que les cinq protéines r de liaison précoce agissent comme des auxiliaires de repliement bien avant que l'ARN 23S complet ne soit transcrit.

Mots Clés

Assemblage de ribosomes, expériences sur une molécule unique, piège optique

Abstract

Double-stranded DNA and RNA (dsDNA, dsRNA) undergo overstretching transitions at forces around 60 pN. We perform force measurements using a dual-beam optical trap that holds two beads linked by a single molecule. One strand of the duplex is attached at both extremities to the beads, while the other strand is attached only at one extremity. Four different cases are compared: dsDNA, dsRNA, RNA-DNA hybrid with DNA under tension, and DNA-RNA hybrid with RNA under tension.

Overstretching occurs for all four duplexes. The most remarkable difference is that dsRNA exhibits a smooth plateau, while the other duplexes show saw-tooth patterns. We find that dsRNA overstretches by a different mechanism and explain why this property could help RNA structures to assemble and play their biological roles.

Overstretching the RNA-DNA hybrid progressively liberates an RNA strand. Structures formed within this nascent RNA are seen in the force signal upon re-annealing. For the first time to our knowledge, we thus mimic and study co-transcriptional RNA folding in an in-vitro assay. Focusing on the early stage of E.coli large ribosomal subunit assembly (domains I-II of 23S rRNA and r-proteins L4, L13, L20, L22, L24), partial re-annealing is observed more frequently with r-proteins than without. Our results indicate that the five early-binding r-proteins act as folding helpers well before the entire 23S RNA is transcribed.

Keywords

Ribosome assembly, single-molecule experiments, optical trap.